May 18, 2015

Abstract

1 Introduction

This study examines the contribution of transient sources to the astrophysical neutrino flux measured by IceCube (HESE flux). The special focus will be placed upon Gamma Ray Bursts (GRBs).

Contrary to most studies which use external GRB triggers from satellites like Swift and Fermi, this result is based on the opposite idea to use neutrinos in order to trigger follow-up observations with Swift and optical telescopes. The disadvantage of this approach is the additional background while the advantage is the 2π field of view (FoV) (northern sky only) and the independence of any gamma-ray sensitivity of the satellites. Instead of using real measured GRBs, a Toy Monte Carlo was written to simulate the neutrino flux from a GRB population up to a redshift of eight. The GRB population and luminosity function is mainly based on a model by Wanderman and Piran (section 4). Other models are included to study the model dependency.

The neutrino signal will be studied on the level of the Optical- and X-Ray Follow Up - O(X)FU - and compared to the measured data. The OFU is described in more detail in section 2.

The GRB population model, simulated GRB neutrinos and experimental results will be combined within the analysis frame work of the GRB population Toy Monte Carlo. It is explained in more detail in section 5 while the main results are summarized and discussed in section 7.

2 Optical- and X-Ray Follow Up

The analysis is based on data from the X-Ray Follow Up including the seasons IC86-1 to IC86-3. It is a system that analyzes data at the South Pole, searching for multiple neutrinos within 100 seconds from one direction (and a possible source location) to trigger Follow-Up observations with various telescopes including the XRT on board the Swift satellite. The latency of such triggers is about three minutes on average. The X-ray Follow-Up (XFU) is a subsystem of the Optical Follow-Up (OFU).

2.1 Alert System

Triggered events are reconstructed at the Pole and evaluated at various levels. They are first roughly classified as possible muons by the Muon Filter ($\sim$40 Hz). Stricter cuts are applied on the OnlineL2Filter, to filter out badly reconstructed events achieving a rate of about 5 Hz. The lower rate allows for further, more detailed reconstructions which are then used for the OFU filter.

The OFU filter is applied to select well reconstructed muon neutrino events from the northern sky. Depending on the season a purity of atmospheric neutrinos of up to 90% was achieved. The filter was improved season to season though the OFU seasons do not match the IceCube seasons. In the first year with the full detector configuration (IC86-1), the OFU system was shut down for several month as the OFU filter didn't work as expected. The debugging took a long time due to multiple software changes that were introduced for IC86-1. For the third OFU season in this analysis a boosted decision tree (BDT) was introduced during the second full IceCube season (IC86-2). As no changes were introduced for IC86-3, the BDT season encompasses the end of IC86-2 and the full IC86-3 IceCube season. The first and last runs of all seasons are listed in Table 1.

Season	IC86-1	IC86-2	IC86-BDT
first run	118691	120156	121788
start date	2011-09-16	2012-05-15	2013-02-01
last run	120155	121787	124701
end date	2012-05-15	2013-02-01	2014-05-06

Table 1: The table lists the different seasons that were analyzed for this work.

The OFU cut selection for the IC86-1 and IC86-2 seasons are based on the following logic

$$\begin{aligned} Zenith(MPE) \geq 90^\circ \ \ and \ \ \frac{logl(MuonLLh)}{NCh-3.5} <= 8 \ \ and \\ \min(Zenith_{Split}) \geq 69.51^\circ \ \ and \\ ((NDir(MPE) \geq 6 \ \ and LDir(MPE) \geq 280) \ \ or \ \ (MuE(MPE) \geq 1e6)) \end{aligned} \tag{2.1}$$

The $Zenith_{Split}$ values refer to the zenith values derived from the topological and time splitter of the events. MPE and MuonLLh refer to the different fit types used to extract the parameters. The cut scheme was completely reworked for IC86-BDT to use a BDT cut.

The single neutrino events passing these cuts are further analyzed to search for multiplets with multiplets consisting of at least two events arriving within the time frame Δt and an angular difference $\Delta\Psi$:

$$\Delta T \leq 100 \text{ s} \ \ and \ \ \Delta\Psi \leq 3.5^\circ \tag{2.2}$$

All seasons have in common that roughly 50 - 60 doublets per year are expected to be generated purely from the background of atmospheric neutrinos while the background of higher multiplets (triplets, quadruplets) is negligible in the order of once every 15 to 20 years. As observation time with the Swift satellite is precious,

it was agreed to send only the seven most promising doublets looking like a signal per year. The evaluation is based on the OFU test statistic (OFUtst)

$$\begin{aligned}\lambda = -2\ln\mathscr{L} = \frac{\Delta\Psi^2}{\sigma_q^2} + 2\ln(2\pi\sigma_q^2) \\ - 2\ln\left(1 - e^{\frac{-\theta_A^2}{2\sigma_w^2}}\right) + 2\ln\left(\frac{\Delta T}{100\,\mathrm{s}}\right)\end{aligned} \tag{2.3}$$

in which the time between the neutrinos in the multiplet is denoted as ΔT and their angular separation as $\Delta\Psi$. $\sigma_q^2 = \sigma_1^2 + \sigma_2^2$ and $\sigma_w^2 = \left(1/\sigma_1^2 + 1/\sigma_2^2\right)^{-1}$ are the combined uncertainties of the directional reconstruction errors σ_1 and σ_2 of the two neutrino events. θ_A corresponds to the (circularized) angular radius of the field of view (FoV) of the follow-up telescope (set to 0.5° for Swift). A cut value λ_{cut} was chosen each season to filter out the best nine alerts (Table 2). The value change with the IC86-BDT season as a higher singlet rate was allowed resulting in more doublets per year. Statistically, two more alerts will be lost because Swift can't observe about 80% of the sky due to the moon and the sun.

Season	IC86-1	IC86-2	IC86-BDT
cut value	-8.8	-8.8	-9.41

Table 2: The cut values on the likelihood to filter down the number of background doublets to less or equal than 9.

The full derivation of the test statistic can be found in the proposal to the IceCube collaboration (reference ???).

2.2 Monitoring

The alert system described in the previous section delivers alerts only if it is operational. To monitor the system an additional kind of alerts were introduced. Test alerts are multiplets formed by neutrino events with a time difference of less than 100 seconds and an angular difference of $3.5 < \Delta\Psi \leq 7.5°$. The events going into the multiplet decision have been selected by applying softer cuts on the Online Level 2 events, i.e. they are more background contaminated than the OFU events. The less stringent cuts and the different condition for the angular difference yield the desired test alert rate of about one test alert every ten minutes and prevent test alerts to be alerts as well. A lack of test alerts indicates problems with either the IceCube detector itself, our alert system, or the communication processes and an alarm is raised after a two hour signal silence.

3 Background Expectation

The previous section described the set up of the X-ray Follow-Up including the expectation of generating alerts based on background events. It is crucial to understand the amount of the false positives to distinguish a possible signal contribution to the alert rate. An average background estimation is obtained by scrambling the neutrino singlets on the level of the Optical Follow-Up Filter.

The neutrino singlets on the level of the Optical Follow-Up Filter consist of about 80 - 90% of atmospheric neutrinos and 10 - 20% of misreconstructed muons. If a signal is present, it will be suppressed in comparison to the background. In the scrambling process the time and reconstruction information are split. While the time structure of the events is being kept in tact, incorporating possible time dependent rate changes, e.g. due to seasonal variations, for each scrambled result, the reconstruction information such as direction and quality is stripped of and randomly attributed to a different event time. An illustration is shown in Figure 1.

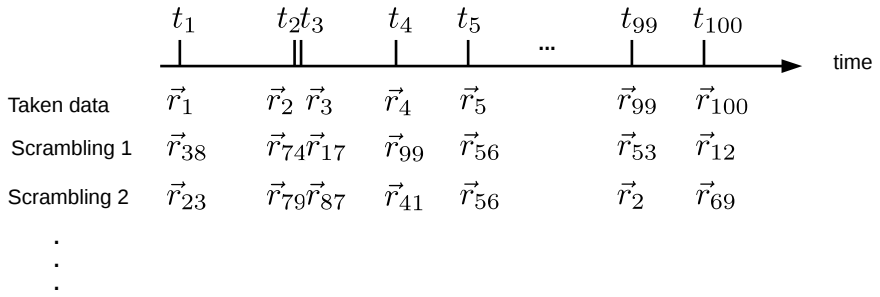

Figure 1: An illustration of the scrambling process for an example of 100 events. The time structure stays the same while the directional information is appointed to a new time randomly with each scrambling.

Events considered in the background estimation should only be events that actually were able to contribute to the triggered alerts, i.e. events detected while the Follow-Up system was operational. Towards that end all OFU singlets were extracted from the database and a time filter developed to exclude events happening during the Follow-Up downtime. There are several factors contributing to downtime. Only data taken during good physics runs are considered. The good-run decision is based on a goodrun list extracted from i3live. The snapshot numbers are listed in Table 3.

Season	IC86-1	IC86-2	IC86-3
snapshot	94	109	93

Table 3: The snapshot numbers of the goodrun lists used for the different seasons.

Any real alert that was triggered during the three years considered in this analysis that occurred during a bad run is excluded in this analysis.

However, the good run list only evaluates the normal function of the IceCube detector but does not include downtime that is isolated to the Follow-Up System. Reasons can be various from software problems only affecting the OFU system to transmission problems via the ITS satellite.

The OFU uptime is evaluated using the test alerts that are designed to monitor the OFU systems. On average, a test alert is expected to arrive every ten minutes. For this analysis, the system is considered 'down' if there is no test alert in a window twenty minutes after a test alert and twenty minutes before the next alert. This procedure averages over the effects that the system might crash directly after a test alert or that a new test alert arrives directly after the restart of the system and that the system is running though no test alerts arrived for over twenty minutes.

Using this time mask, all online alerts could be reproduced by re-analyzing the data offline and no new alerts were found. On average, 5.4, 6.5 and 5.7 Swift doublets were expected during the different seasons

Season	IC86-1	IC86-2	IC86-BDT
livetime [d]	233.56	235.42	407.38
uptime [%]	0.91	0.90	0.89
expected Swift	5.42	6.49	5.7
measured Swift	6	5	7
expected multiplets	0.044	0.063	0.073
measured multiplets	0	0	0

Table 4: The table lists both the uptime of the Optical Follow-Up system and the results of the data scrambling to estimate the average background rate. The measured values are documented here for comparison.

while the higher multiplet rate expectation varies between 0.044 and 0.073 (Table 4). An example of the scrambled distributions of expected Swift alerts during the IC86-1 season can be seen in Figures 2a and 2b.

The OFU system had an average uptime of 90%. This includes downtime for OFU unrelated reasons like calibration runs.

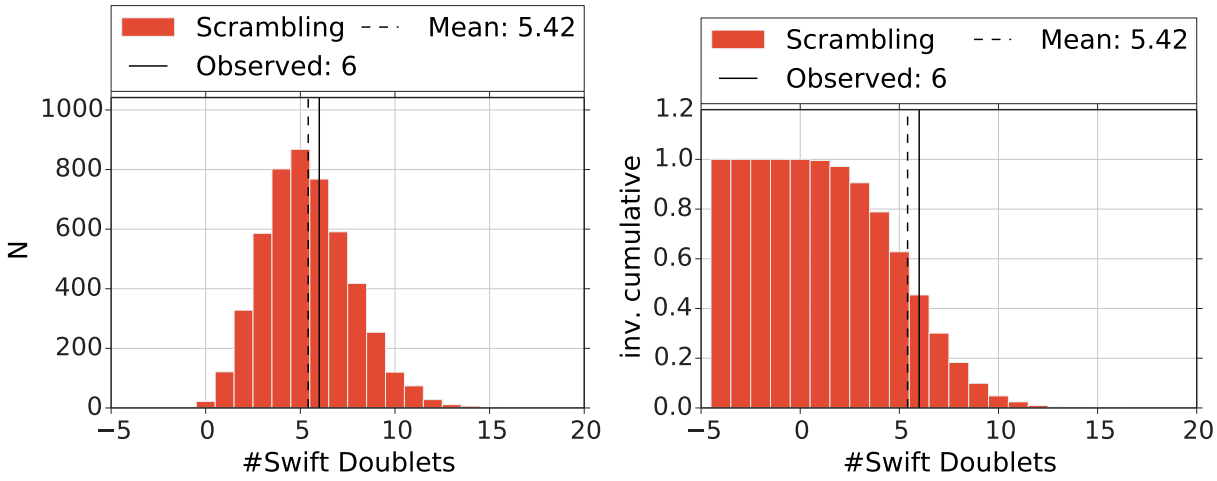

(a) The differential distribution

(b) The inverse cumulative distribution.

Figure 2: The differential and inverse cumulative distributions of detectable Swift doublets for a hundred thousand scrambled datasets. The distributions for IC86-1 is chosen as an example.

4 GRB models

Most GRB analysis within IceCube use information from observed GRBs to look for neutrino clusters in time and space correlated to the detected GRBs. This strategy has the obvious advantage of reducing the neutrino background to achieve higher significance per GRB observation. However, due to the limited Field of View of the satellites there will be many GRBs that stay undetected. Furthermore, one is biased by the detection sensitivity of the satellites.

In this analysis, a GRB population is assumed based on theoretical work and extrapolation based on data from Swift and other satellites. The redshift and luminosity functions are extracted. The neutrino luminosity function is assumed to have the same shape and is shifted in energy by an efficiency factor ε (see section 5.5). The different population models under consideration are discussed in this chapter.

The main analysis has been done based on the luminosity function and GRB rate density calculated by Wanderman and Piran (4.2). The other models presented here were considered to examine the dependency on the assumed model.

4.1 Cosmology

The following cosmological definitions are used in the calculations of the following chapters.

Differential co-moving shell volume

$$dV = 4\pi D_H \frac{(1+z)^2 D_a^2(z)}{K(z)} dz \tag{4.1}$$

Hubble distance

$$D_H = \frac{c}{H_0} = 3000 h^{-1}\text{Mpc} \tag{4.2}$$

Angular distance

$$D_a(z) = (1+z)^{-2} D_l(z) \tag{4.3}$$

Parameters

- $K(z) = \sqrt{\Omega_m (1+z)^3 + \Omega_\Lambda}$
- $h = 0.7$
- $\Omega_m = 0.3$
- Ω_Λ

4.2 Wanderman Piran

Wanderman and Piran (4) extracted a GRB distribution in redshift and luminosity using GRB data up to 2009 applying detection efficiencies for both the detection in γ- rays and a following determination of the host redshift, i.e., the redshift of the GRB.

The differential co-moving rate of bursts (fig. 3b) at a redshift z is

$$R(z) = \frac{R_{\text{GRB}}(z)}{(1+z)} \frac{dV(z)}{dz} \tag{4.4}$$

$dV(z)/dz$ is the differential co-moving shell volume and the factor $(1+z)^{-1}$ reflects the cosmological time dilation. R_{GRB} is fitted to data with the result (Fig 3a)

$$R_{\text{GRB}}(z) = \begin{cases} \rho_0 \cdot (1+z)^{n_1} & z \leq z_1 \\ \rho_0 \cdot (1+z_1)^{n_1 - n_2} (1+z)^{n_2} & z > z_1 \end{cases} \tag{4.5}$$

with $n_1 = 2.07$, $n_2 = -1.36$, $z_1 = 3.11$ and the local rate $\rho_0 = 1.25\text{Gpc}^{-3}\text{yr}^{-1}$.

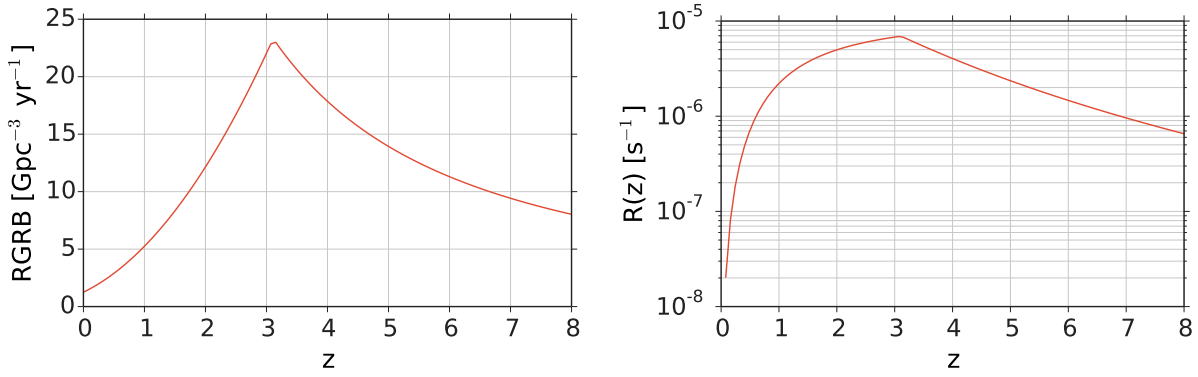

(a) Derived RGRB function (WP)

(b) Differential co-moving rate

Figure 3: The distribution of GRBs over the redshift displaying the derived RGRB function and the differential co-moving rate.

The peak γ-luminosity at the source L_{Peak} (Fig. 4) is determined to follow

$$\Phi(L_{\text{Peak}}) = \begin{cases} \left(\frac{L}{L_*}\right)^{-\alpha} & L < L_* \\ \left(\frac{L}{L_*}\right)^{-\beta} & L > L_* \end{cases} \tag{4.6}$$

in which $\log_{10} L_* = 52.53$ erg / s is the break luminosity and $\alpha = 0.17$ and $\beta = 1.44$ are the spectral indices (Table 5). No redshift evolution of the luminosity is assumed.

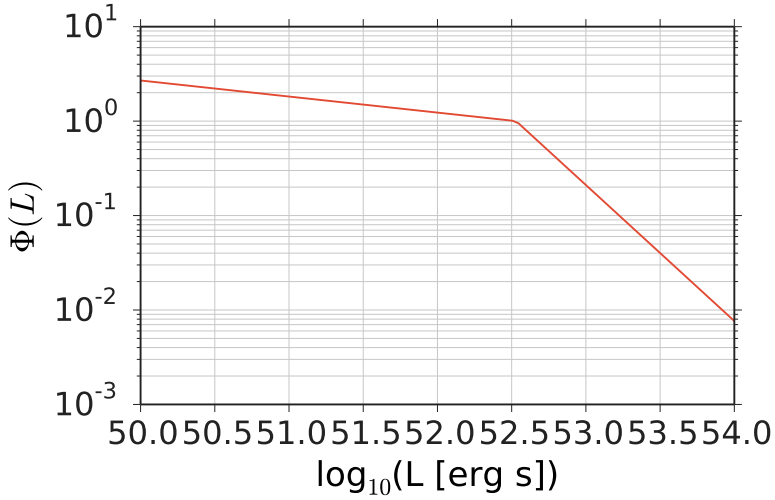

Figure 4: The luminosity function derived in the WP model. (deleted this figure and use the one including HC?)

4.3 Howell Coward

There is a more recent work (2) by Howell, Coward, Stratta, Gendre and Zhou basing the redshift distribution on the same general shape as Wanderman Piran and testing various luminosity functions. For purposes of readability it will be called Howell-Coward or HC-model. One of the tested luminosity functions will be compared to the model by Wanderman and Piran (WP).

Model	$\log_{10}\left(L_*\left[\text{erg s}^{-1}\right]\right)$	α	β	$\rho_0\left[\text{Gpc}^{-3}\ \text{yr}^{-1}\right]$	z_1	n_1	n_2	N_{GRB}
WP	52.53	0.17	1.44	1.25	3.11	2.07	-1.36	9082.83
HC	51.7	0.13	2.42	0.48	3.6	2.1	-0.7	4791.97

Table 5: Fit parameters to the luminosity functions and redshift distributions of the tested models.

Similarly to Wanderman and Piran, the luminosity is assumed to not evolve with redshift in their main work. The same functions as in WP are used for redshift distribution (eq. 4.5) and the luminosity function (Eq. 4.6), but different fit results were obtained for the parameters (Table 5).

The considered luminosity range is with $\log_{10}L_{\text{Peak}} \in (49,54)$ larger than in WP ($\log_{10}L_{\text{Peak}} \in (50,54)$). The break peak luminosity is lower than in WP transitioning into a harder slope towards higher luminosities (Fig. 5). At lower luminosities the slopes of HC and WP are quite similar (0.13, 0.17) leading to more low luminosity GRBs in HC due to the greater range.

The redshift distributions rise to the break redshift quite similarly although the break is at higher redshifts (3.6 compared to 3.11) for HC transitioning into a slower decay at large z. The overall impact are more distant GRBs in HC than in WP which should lead to a slight weakening of the limits.

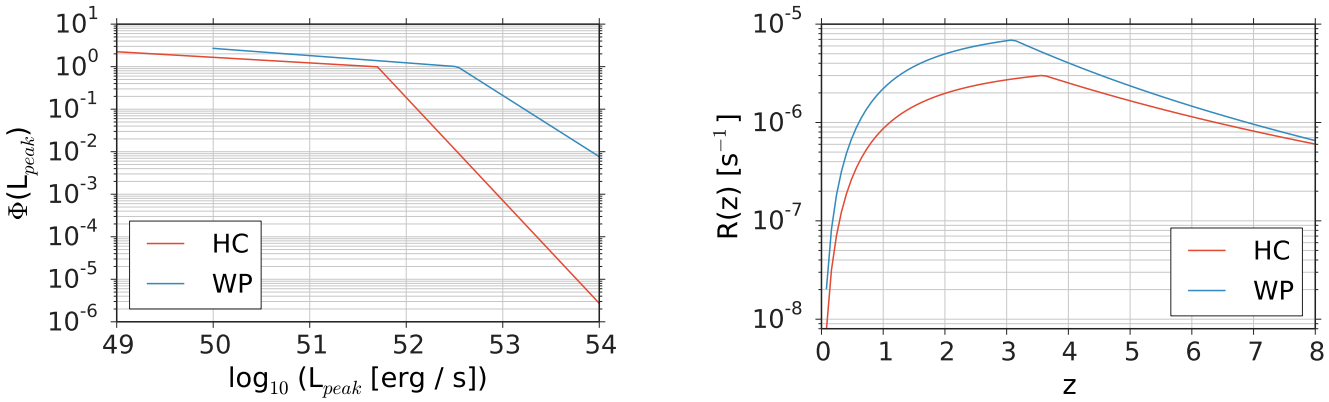

(a) Luminosity functions

(b) Redshift distributions

Figure 5: The luminosity functions (left) from the Wanderman-Piran model and two functions from the HC model on the left. The WP only take into account luminosities in the range of $10^{50} - 10^{54}$ erg / s which is reflected in the shorter blue line.
The redshift distributions (right) develop similar up to $z = 3.11$ at which point it breaks for the WP-model. The HC predicts more GRBs at higher redshift values.

4.4 Long low luminosity GRBs

In recent years, IceCube has started to rule out the first optimistic GRB neutrino emission models leading to new ideas as to possible neutrino emitters. It has been proposed (3) that a high number of very low luminosity GRBs exists that are difficult to detect in γ-rays, but could produce most of the neutrinos expected from GRBs. In principle, the follow-up analysis based on IceCube triggers can be an approach to examine these objects. Thus, they are mentioned here briefly for the sake of completeness and future possible Follow-Up extensions.

Unfortunately, these low luminosity GRBs are predicted to have a prompt emission phase in the range of 10^3 s. The follow-up program suppresses background by allowing a maximal time difference of 100s between two events reducing the sensitivity to very long GRBs at the same time. Therefore, they have not been examined yet within this analysis but mentioned for the interested reader.

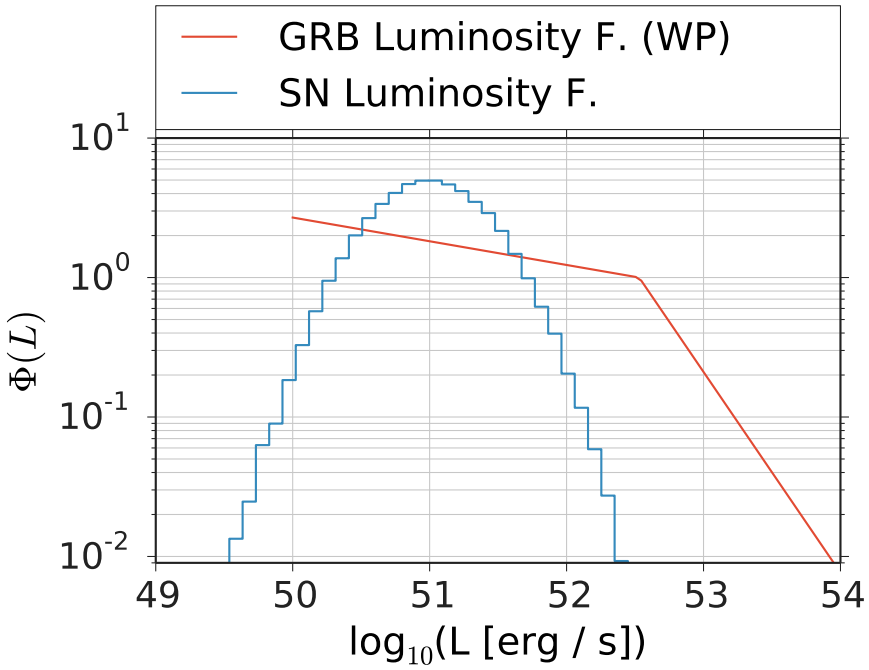

Figure 6

4.5 Supernovae

The models presented described GRB population models. However, the Optical Follow-Up is sensitive to all short ($O(10\text{ s})$) transient neutrino sources. E.g. the simulation can be used to examine a population of core collapse Supernovae (SNe) as well. A model predicting high energy neutrinos from SNe (1) assumes a jet production withing the SN similar to the jets of the GRB fireball model. Due to the lack of energy, they do not penetrate the stellar envelope and are therefore invisible to the telescopes observing the electromagnetic signal. In contrast, neutrinos would escape the SN and could possibly be detected within IceCube. The exact mechanism and resulting predicted spectrum is not important for this analysis as we assume a population of sources and attribute to them a spectrum that reproduces the measured HESE flux.

SNe follow the star formation rate which, in first order, can be approximated by the Wanderman Piran redshift distribution. However, the luminosity function differs quite a bit by not showing the big variations in luminosity that are observed for GRBs. Instead, the luminosity function is assumed to follow a Gaussian curve in logarithmic space with a width of 0.4 orders of magnitudes corresponding to a width of one astronomical magnitude. A comparison to the WP luminosity function is shown in Figure 6. The mean luminosity is chosen at random and will be later adjusted to create the expected neutrino flux.

4.6 Duration

Ninety percent of the detectable γ-ray flux is received between a time intervall called t_{90}. The Swift GRB table [1] lists values for most GRBs. The extracted values for long GRBs are displayed in figure 7.

In the GRB Toy Monte Carlo t_{90} values will be drawn at source (marked with$\hat{}$) to calculate the total energy output according to

$$P(\hat{t}_{90}) = a \cdot \exp\left(-\frac{(\hat{t}_{90}-b)^2}{2c^2}\right). \tag{4.7}$$

It will be folded with the drawn redshift to calculate the t_{90} pervieved at earth.

$$t_{90} = \hat{t}_{90} \cdot (1+z) \tag{4.8}$$

[1] http://swift.gsfc.nasa.gov/archive/grb_table/

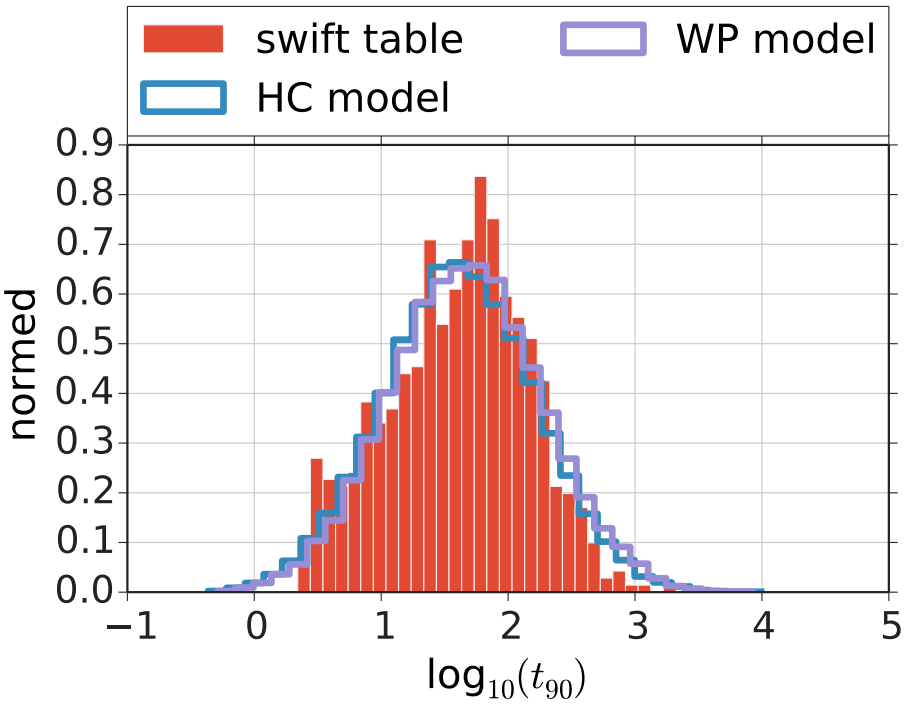

Figure 7: The t_{90} distributions at earth based on data extracted from the Swift database (reference ???) and the drawn distributions based on t_{90} values drawn at source and folded with the redshift distributions.

The t_{90} distributions for the WP and HC models are displayed in figure 7 as well.

5 GRB Toy Monte Carlo

The previous chapters have laid the ground work on which the GRB Population Toy Monte Carlo is built. This chapter describes how GRBs are being drawn according to the models described in section 4 and how the neutrino signal expectation within IceCube is calculated. The analysis will then test to which extent certain transient populations can reproduce the detected HESE flux.

5.1 GRB Spectra

The astrophysical neutrinos discovered by IceCube can be described by various spectra depending on the data and conditions set for the fit. This analysis examines three different scenarios.

The first two scenarios are based on global fits not only to the HESE events but to other datasets as well. Once a fit with a cut-off was chosen and once the index of the power law was free. The third fit is exclusively based on the HESE data with a free index:

Global fit: cut-off

$$E^2\Phi = 0.9 \cdot 10^{-8} \cdot \exp\left(-\frac{E}{2.8\ \text{PeV}}\right) \text{GeV s}^{-1}\ \text{sr}^{-1}\ \text{cm}^{-2} \tag{5.1}$$

Global fit: free index

$$E^2\Phi = 2.24 \cdot 10^{-8} \left(\frac{E}{100\ \text{PeV}}\right)^{-0.7} \cdot \exp\left(-\frac{E}{2.8\ \text{PeV}}\right) \text{GeV s}^{-1}\ \text{sr}^{-1}\ \text{cm}^{-2} \tag{5.2}$$

HESE fit: free index

$$E^2\Phi = 1.5 \cdot 10^{-8} \left(\frac{E}{100\ \text{PeV}}\right)^{-0.3} \cdot \exp\left(-\frac{E}{2.8\ \text{PeV}}\right) \text{GeV s}^{-1}\ \text{sr}^{-1}\ \text{cm}^{-2} \tag{5.3}$$

For the purpose of this analysis, these spectra are assumed to be created by GRBs or other examined transient sources and as such a superposition of the individual GRB spectra. They are given the same shape. Generally, the flux follows the following formula which will be used in the following chapters for general calculations.

$$\Phi = \Phi_0 E^{-\gamma} \exp\left(-\frac{E}{\hat{E}_{cut}}\right) \tag{5.4}$$

The break energy $\hat{E}_{cut}$ is set to be a physics parameter that is the same for all GRBs. In case of scenario 1 it has to be optimized to reproduce the cut-off at earth of 2.8 PeV as good as possible. In the other two cases it is set to 10^{20} GeV and doesn't have any impact within the further analysis.

5.2 Drawing GRB properties

This section describes how properties such as the luminosity and the redshift are drawn according to their distribution ($f1$) specified in section 4.

The function determines the maximum f_{max} and minimum f_{min} of $f1$ within a range in which a parameter p is to be drawn. The range is specified by the user.

In the next step it randomly throws a value $p1$ for p within the specified range and a random value f_{random} between f_{min} and f_{max}. Is $f_{random} <= f(p1)$ fullfilled, then p1 is returned as a value for p according to the distribution $f1$. Otherwise the step is repeated until the condition is met.

The following parameters are drawn:

- Peak luminosity L_{Peak}
- Redshift z
- Zenith angle θ (uniform in $\cos(\theta)$)
- Azimuth angle ϕ (uniform)
- $t_{90,S}$

5.3 Number of expected Neutrinos based on NuGen Datasets

The simulation uses NuGen datasets to calculate the number of expected neutrinos according to the standard formula.

$$N^{\nu}_{\text{exp}} = \sum_i \frac{dF_P(E_i)}{dE_i} \cdot \frac{OneWeight_i}{N_{\text{generated}}} \tag{5.5}$$

The nugen simulation describes the probability for each simulated neutrino event i to reach the detector, interact within its effective volume and to be detected ($OneWeight_i$), the individual energy E_i and the number of generated MC neutrino events $N_{\text{generated}}$.

The differential particle fluence $\frac{dF_P}{dE}$ at earth needs to be calculated based on the GRB properties drawn at source - peak luminosity $\hat{L}_{\text{Peak}}$, $\hat{t}_{90,S}$, redshift (sections 5.4.1 - 5.4.3). Values at source are marked with a hat while values on earth are represented by the appropriate characters themselves.

5.3.1 Zenith Bands

The probability to detect a neutrino is highly dependent on the zenith angle of its origin. The number of expected neutrinos within IceCube can be calculated for all simulated events (eq. 5.5). However, these are distributed over the whole sky and might not represent a GRB from a specific zenith direction very well. Therefore, only events from a zenith region around a drawn GRB direction will be used to calculate the expected signal. The true direction of each considered event needs to be within a range around the GRB direction in CosΘ

$$\text{Cos}\left(\Theta_{\nu,\text{true}}\right) \in \left[\text{Cos}\left(\Theta_{\text{GRB}}\right) - ZBW, \text{Cos}\left(\Theta_{\text{GRB}}\right) + ZBW\right] \tag{5.6}$$

The zenith band width is set to $ZBW = 0.05$ and equal in cosinus of the zenith angle to achieve similar (and enough) statistics near pole and horizon.

Consequently, the number of expected neutrino events within the detector (eq. 5.5) is not calculated anymore based on the total number of generated events $N_{\text{generated}}$ over the whole sky but only a fraction of events within the zenith band. Therefore, $N_{\text{generated}}$ needs to be replaced by an effective number of generated events

$$N^{\text{eff}}_{\text{generated}} = N_{\text{generated}} \cdot \frac{A_{ZB}}{4\pi} \tag{5.7}$$

in which A_{ZB} is the area of the zenith band. The number of expected neutrinos is then

$$N^{\nu}_{\text{exp}} = \sum_i \frac{dF_P(E_i)}{dE_i} \cdot \frac{OneWeight_i}{N^{\text{eff}}_{\text{generated}}} = \sum_i \frac{dF_P(E_i)}{dE_i} \cdot \frac{OneWeight_i}{N_{\text{generated}} \cdot \frac{A_{ZB}}{4\pi}} \tag{5.8}$$

5.4 Shifting Event Positions to GRB position

In later steps the directions of different neutrino events will be compared to each other. Therefore, all events within a zenith band are shifted such that their true direction will coincide with the GRB direction and the shifted or new reconstructed direction keep the same distance and direction to the GRB direction.

5.4.1 Total Emitted Energy as Source $\hat{E}_{\nu,\text{total}}$

So far, the steps dealing with simulation effects and neutrino directions have been described. To calculate N_{exp}^{ν} the differential particle fluence in energy at earth needs to be calculated as well, based on parameters that are drawn as part of the simulation (chapter 5.2). A first step is to calculate the total emitted energy in neutrinos at the source $\hat{E}_{\nu,\text{total}}$.

The peak luminosity and the 90% time window can be used if the light curve is known. In this work a fast rise and rapid decay (FRED) light curve with an instant jump to the peak luminosity and an exponential decay afterwards is assumed.

The luminosity at a given time $\hat{t}$ is defined as

$$\hat{L}(\hat{t}) = \hat{L}_{\text{Peak}} \cdot e^{\left(-\frac{\hat{t}}{\hat{\tau}}\right)} \tag{5.9}$$

The total energy is the time integral over the time dependent luminosity distribution

$$\begin{aligned} \hat{E}_{\nu,\text{total}} &= \int_0^{\infty} \hat{L}(\hat{t}) d\hat{t} = \hat{L}_{\text{Peak}} \int_0^{\infty} e^{-\frac{t}{\tau}} dt \\ &= -\hat{\tau} \cdot \hat{L}_{\text{Peak}} \left[e^{-\frac{\hat{t}}{\hat{\tau}}} \right]_0^{\infty} = \hat{\tau} \cdot \hat{L}_{\text{Peak}} \end{aligned} \tag{5.10}$$

The final shape of the distribution depends on the unknown τ which needs to be replaced by a known quantity such as the 90 % time window $\hat{t}_{90}$ in which 90% or $\hat{E}_{\nu,90} = 0.9 \cdot \hat{E}_{\nu,\text{total}}$ are observed. The amount of energy radiated within this time can be determined with

$$\begin{aligned} \hat{E}_{\nu,90} = 0.9 \cdot \hat{E}_{\nu,\text{total}} = 0.9 \cdot \hat{\tau} \hat{L}_{\text{Peak}} &= \int_0^{\hat{t}_{90}} \hat{L}(\hat{t}) d\hat{t} \\ = -\hat{\tau} \hat{L}_{\text{Peak}} \left[e^{-\frac{\hat{t}}{\hat{\tau}}} \right]_0^{\hat{t}_{90}} &= \hat{\tau} \hat{L}_{\text{Peak}} \left[1 - e^{-\frac{\hat{t}_{90}}{\hat{\tau}}} \right] \end{aligned} \tag{5.11}$$

leading to

$$\begin{aligned} \left[1 - e^{-\frac{\hat{t}_{90}}{\hat{\tau}}} \right] &= 0.9 \\ 0.1 &= e^{-\frac{\hat{t}_{90}}{\hat{\tau}}} \\ \ln(0.1) &= -\frac{\hat{t}_{90}}{\hat{\tau}} \\ \Rightarrow \hat{\tau} &= \frac{-\hat{t}_{90}}{\ln(0.1)} \end{aligned} \tag{5.12}$$

Entering this in equation 5.10 leads to:

$$\hat{E}_{\nu,\text{total}} = -\hat{L}_{\text{Peak}} \frac{\hat{t}_{90}}{\ln(0.1)} \tag{5.13}$$

5.4.2 Fluence at Source

The simulation draws GRB properties at source. In the first step they are used to calculate the differential particle fluence in energy $\frac{d\hat{F}_P}{d\hat{E}}$ in units $\text{GeV}^{-1}\text{s}^{-1}\text{sr}^{-1}\text{cm}^{-2}$ at a small co-moving distance from the source $\hat{d}_0$. The spectral shape is a generalization based on the fits to the HESE flux (eq. 5.4).

$$\frac{d\hat{F}_P}{d\hat{E}} = \frac{\hat{F}_0}{4\pi\hat{d}_0^2} \cdot \hat{E}^{-\gamma} \exp\left(-\frac{\hat{E}}{\hat{E}_{\text{cut}}} \right) \tag{5.14}$$

The fluence normalization $\hat{F}_0$ is unknown. However, in the previous section 5.4.1 the total emitted energy was calculated. It equals the integral over $\hat{E} \cdot \frac{d\hat{F}_P}{d\hat{E}}$.

$$\hat{E}_{\nu,\text{total}} = \int_{\hat{E}_{min}}^{\infty} \hat{E}\hat{F}_0\hat{E}^{-\gamma}\exp\left(-\frac{\hat{E}}{\hat{E}_{\text{cut}}}\right)d\hat{E} = \hat{F}_0\Upsilon\left(\hat{E}_{min},\hat{E}_{\text{cut}}\right) \tag{5.15}$$

The result depends on two GRB parameters which are chosen equally as physics parameters for all GRBs: A minimal energy of the neutrinos $\hat{E}_{min}$ and the break energy $\hat{E}_{cut}$. Once, these parameters are chosen, Υ is a constant for all GRBs and the differential particle fluence in energy at source can be written as

$$\frac{d\hat{F}_P}{d\hat{E}} = \frac{\hat{E}_{\nu,\text{total}}}{4\pi d_0^2\Upsilon\left(\hat{E}_{min},\hat{E}_{\text{cut}}\right)} \cdot \hat{E}^{-\gamma}\exp\left(-\frac{\hat{E}}{\hat{E}_{\text{cut}}}\right) \tag{5.16}$$

5.4.3 Fluence at Earth

Having derived the fluence at source, cosmological effects need to be taken into account when calculating the fluence at earth. The energy and time at source relate to the values at earth with $\hat{E} = (1+z)E$ and $\hat{t} = \frac{t}{1+z}$. The energy flux at earth Φ_E is linked to the luminosity via

$$\Phi_E(t) = \frac{\hat{L}\left(\hat{E},\hat{t}\right)}{4\pi d_l^2} = \frac{L(E,t)}{4\pi d_l^2} \tag{5.17}$$

with the luminosity distance $d_l = (1+z)\cdot d_c$. The particle fluence F_P at earth is the time integrated particle flux Φ_P which in turn is the energy derivative of the energy flux.

$$F_P(E) = \int \Phi_P(E,t)\,dt = \int \frac{d\Phi_E(E,t)}{dE}\,dt \tag{5.18}$$

The energy flux can be replaced with the luminosity according to 5.17. Applying a derivation in energy and transforming energy and time to the source frame, one obtains

$$\begin{aligned}
\frac{dF_P(E)}{dE} &= \frac{1}{4\pi d_l^2}\int \frac{d^2L(t)}{dE^2}dt && (5.19)\\
&= \frac{1}{4\pi d_l^2}\int \frac{d^2L(\hat{t})}{d\hat{E}^2}\frac{d^2\hat{E}}{dE^2}\frac{dt}{d\hat{t}}d\hat{t} && (5.20)\\
&= \frac{(1+z)^3}{4\pi d_l^2}\int \frac{d^2L(\hat{t})}{d\hat{E}^2}d\hat{t} && (5.21)
\end{aligned}$$

A similar equation is true for differential particle fluence in energy near the source at a distance d_0.

$$\frac{d\hat{F}_P(\hat{E})}{d\hat{E}} = \frac{1}{4\pi d_0^2}\int \frac{d^2L(\hat{t})}{d\hat{E}^2}d\hat{t} \tag{5.22}$$

Combining equation 5.21 and 5.22 relates the differential particle fluence at earth to the differential particle fluence at source derived in 5.16.

$$\begin{aligned}
\frac{dF_P(E)}{dE} &= \left(\frac{d_0}{d_l}\right)^2(1+z)^3\frac{d\hat{F}_P(\hat{E})}{d\hat{E}} && (5.23)\\
&= \frac{\hat{E}_{\nu,\text{total}}}{4\pi d_l^2\Upsilon\left(\hat{E}_{min},\hat{E}_{\text{cut}}\right)} \cdot \hat{E}^{-\gamma}\exp\left(-\frac{\hat{E}}{\hat{E}_{\text{cut}}}\right)\cdot(1+z)^3 && (5.24)\\
&= \frac{\hat{E}_{\nu,\text{total}}}{4\pi d_l^2\Upsilon\left(\hat{E}_{min},\hat{E}_{\text{cut}}\right)} \cdot E^{-\gamma}\exp\left(-\frac{E\cdot(1+z)}{\hat{E}_{\text{cut}}}\right)\cdot(1+z)^{3-\gamma} && (5.25)
\end{aligned}$$

In the last step the energy at source was replaced with the energy at earth in consideration of the cosmological effects. This formula can now be used to calculate the number of expected neutrinos within IceCube given the drawn properties and a nugen dataset (section 5.4.4).

5.4.4 Number of Expected Neutrinos Within IceCube

This chapter described how the differential particle fluence in energy can be derived from the drawn parameters describing a GRB in this simulation. The number of expected neutrinos is given with

$$\begin{aligned} N^{\nu}_{\text{exp}} &= \sum_i \frac{dF_P(E_i)}{dE} \cdot \frac{OneWeight_i}{N_{\text{generated}} \cdot A_{ZB}} \\ &= \sum_i \cdot \frac{\hat{E}_{\nu,\text{total}}}{4\pi d_l^2 \Upsilon\left(\hat{E}_{min}, \hat{E}_{\text{cut}}\right)} \cdot E_i^{-\gamma} \exp\left(-\frac{E_i \cdot (1+z)}{\hat{E}_{\text{cut}}}\right) \cdot (1+z)^{3-\gamma} \frac{OneWeight_i}{N_{\text{generated}} \cdot \frac{A_{ZB}}{4\pi}} \end{aligned} \tag{5.26}$$

It is dependent on various factors of the nugen simulation and some parameters from the derivation of the differential particle fluence. The nugen simulation describes the probability for each simulated event i to reach the detector, interact within its effective volume and to be detected ($OneWeight_i$), the individual energy E_i, the number of generated MC neutrino events $N_{\text{generated}}$ and a re-weighting factor $\frac{A_{ZB}}{4\pi}$. The re-weighting factor has been explained in more detail in section 5.3.1.

Furthermore, the number of expected neutrinos is dependent on the redshift of the GRB, the total emitted energy in neutrinos $\hat{E}_{\nu,\text{total}}$ - and thus $\hat{L}_{\text{Peak}}$ and $\hat{t}_{90}$ - as well as the constant Υ. The constant itself is dependent on the energy of the cut-off $\hat{E}_{\text{cut}}$ and the minimal neutrino energy at source $\hat{E}_{min}$. As described in 5.1 the cut-off energy will be optimized to reproduce the observed cut-off or set to very high values depending on the spectrum that is used. The effect of the minimal energy can be absorbed into the normalization to the HESE flux (chapter 5.5). The complete impact is studied in chapter 7.

5.5 Normalization to HESE Flux

The luminosity is drawn according to the luminosity function fitted to gamma-ray data, assuming the neutrino luminosity function to follow the same shape. However, a normalization factor might be needed to restrict it to the correct energies and consequently to the correct number of neutrinos to produce the HESE flux. ($N^{\nu}_{\text{exp}} \propto \hat{E}_{\nu,\text{total}} \propto L_{\text{Peak}}$). Equation 5.8 evolves to

$$N^{\nu}_{\text{exp}} = \varepsilon \cdot \sum_i \cdot \frac{\hat{E}_{\nu,\text{total}}}{4\pi d_l^2 \Upsilon\left(\hat{E}_{min}, \hat{E}_{\text{cut}}\right)} \cdot E_i^{-\gamma} \exp\left(-\frac{E_i \cdot (1+z)}{\hat{E}_{\text{cut}}}\right) \cdot (1+z)^{3-\gamma} \frac{OneWeight_i}{N_{\text{generated}} \cdot \frac{A_{ZB}}{4\pi}} \tag{5.27}$$

$$= \varepsilon^* \cdot \sum_i \cdot \frac{\hat{E}_{\nu,\text{total}}}{4\pi d_l^2} \cdot E_i^{-\gamma} \exp\left(-\frac{E_i \cdot (1+z)}{\hat{E}_{\text{cut}}}\right) \cdot (1+z)^{3-\gamma} \frac{OneWeight_i}{N_{\text{generated}} \cdot \frac{A_{ZB}}{4\pi}} \tag{5.28}$$

Once $\hat{E}_{min}$ (chapter ???) and $\hat{E}_{\text{cut}}$ are determined, Υ is a constant for every GRB which can be included in an effective normalization factor

$$\varepsilon^* = \frac{\varepsilon}{\Upsilon\left(\hat{E}_{min}, \hat{E}_{\text{cut}}\right)} \tag{5.29}$$

Due to the effective normalization factor it is redundant to calculate the constant Υ. However, a different ε^* needs to be determined for different $\hat{E}_{min}$. The impact of choosing different minimal energies is studied in chapter ???.

There are two ways to determine ε - a Monte Carlo based method and a semi-analytic one.

5.5.1 ε^* - Monte Carlo Based

This approach was followed by Nora Strotjohann. Given the different spectra fitted to the HESE flux (chapter 5.1), a different number of neutrinos per year are expected due to GRBs. Using the NuGen simulation without the GRB simulation, one can simply calculate the number of neutrinos using the spectra fitted at earth. They are displayed in figure 8. Their shape is quite similar at high energies at which the HESE

events were found. However, the curves diverge quite significantly at lower energies leading to different predictions about the number of neutrinos one could expect from GRBs on OFU level.

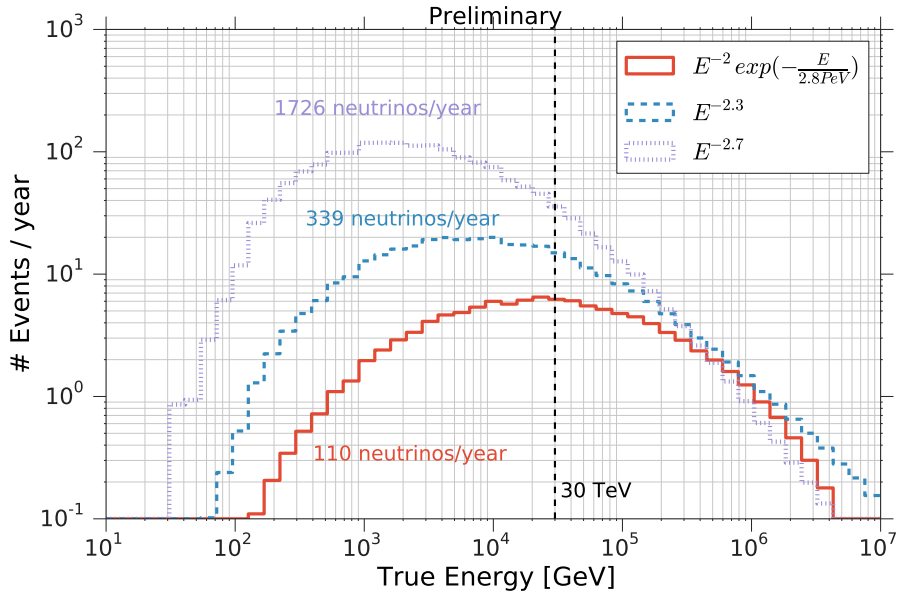

Figure 8: The three different spectra fitted to the HESE events on OFU level. The true neutrino energy is used. The number of expected neutrinos is highly dependent on the chosen spectrum.

To determine ε^* up to 5 million GRBs ($N_{\text{GRB, sim}}$) are simulated with ε^* set to one. The sum over N^{ν}_{exp} of all GRBs is renormalized to the number of expected GRBs per year $N_{\text{GRB, yr}}$ and needs to reproduce the number of expected neutrinos on OFU level.

$$\varepsilon^* = \frac{N^{\nu}_{\text{exp}}(\varepsilon^* = 1) \cdot \frac{N_{\text{GRB, yr}}}{N_{\text{GRB, sim}}}}{N^{\nu}_{\text{exp, OFU}}} \tag{5.30}$$

The final result depends on the number of expected GRBs per year which is an uncertain number. Fortunately, it is a linear factor and ε^* can be changed easily with the knowledge with which $N_{\text{GRB, yr}}$ it was calculated.

$$\varepsilon^*_{\text{new}} = \varepsilon^* \cdot \frac{N^{\text{new}}_{\text{GRB, yr}}}{N_{\text{GRB,yr}}} \tag{5.31}$$

5.5.2 ε^* - Semi-Analytic Approach

The second approach integrates over the expected differential fluxes in energy from all GRBs up to the maximal chosen redshift ($z_{max} = 8$) under consideration of their redshift distribution.

$$\Phi_{\text{GRB}} = \int_{z=0}^{z=8} dz R(z) \cdot \frac{dF_P\left(z, E, \hat{E}_{\nu,\text{total}}\left(\hat{t}_{90}, L_{\text{Peak}}\right)\right)}{dE} \tag{5.32}$$

$$= \int_{z=0}^{z=8} dz R(z) \cdot \frac{\hat{E}_{\nu,\text{total}}}{4\pi d_l^2(z)} \cdot E_i^{-\gamma} \exp\left(-\frac{E_i \cdot (1+z)}{\hat{E}_{\text{cut}}}\right) \cdot (1+z)^{3-\gamma} \tag{5.33}$$

The final result needs to equal the measured fluxes on earth over the whole energy range and the flux is recalculated for 100 energy values between 10 and 10^9 GeV evenly spaced in log$E$.

Next to the redshift of the GRBs and the energy of the neutrinos the signal expectation is dependent on the total energy in neutrinos and thus the peak luminosity and the $\hat{t}_{90}$ values. The average value is calculated

based on an average time window and peak luminosity. The average time window $< \hat{t}_{90} >$ was determined out of 5 million drawn values while the average peak luminosity is calculated according to

$$\begin{aligned} < L_{\text{Peak}} > &= \frac{\int_{L_{\text{Peak}}^{min}}^{L_{\text{Peak}}^{max}} L_{\text{Peak}} \cdot \Phi(L_{\text{Peak}}) d\log_{10} L_{\text{Peak}}}{\int_{L_{\text{Peak}}^{min}}^{L_{\text{Peak}}^{max}} \Phi(L_{\text{Peak}}) d\log_{10} L_{\text{Peak}}} \\ &= \frac{\int_{L_{\text{Peak}}^{min}}^{L_{\text{Peak}}^{max}} L_{\text{Peak}} \cdot \frac{\Phi(L_{\text{Peak}})}{L_{\text{Peak}} \ln(10)} dL_{\text{Peak}}}{\int_{L_{\text{Peak}}^{min}}^{L_{\text{Peak}}^{max}} \frac{\Phi(L_{\text{Peak}})}{L_{\text{Peak}} \ln(10)} dL_{\text{Peak}}} \\ &= \frac{\int_{L_{\text{Peak}}^{min}}^{L_{\text{Peak}}^{max}} \frac{\Phi(L_{\text{Peak}})}{\ln(10)} dL_{\text{Peak}}}{\int_{L_{\text{Peak}}^{min}}^{L_{\text{Peak}}^{max}} \frac{\Phi(L_{\text{Peak}})}{L_{\text{Peak}} \ln(10)} dL_{\text{Peak}}} \end{aligned} \tag{5.34}$$

The co-moving rate density $R(z)$ includes a normalization to the number of expected GRBs according to the used model. If a different number of GRBs is assumed, then the resulting flux needs to be adjusted by an appropriate factor.

This flux of all GRBs up to a redshift of eight needs to reproduce the HESE flux over the whole energy range (Fig. 9a). This can be achieved for the two spectra without a cut-off. However, the HESE flux can not be reproduced at very high energies using the same exponential cut-off for all GRBs at all redshifts. $\hat{E}_{\text{cut}}$ was chosen such that an exact agreement was reached for the most part of the energy range accepting a disagreement in the tail. Possibly, one could determine an energy dependent ε^*. However, given the few numbers of events at these energies and the lack of knowledge of the exact shape of the cut-off due to missing HESE statistic this extra complication was not attempted.

$$\varepsilon^* = \frac{\Phi_{\text{HESE}}(E)}{\Phi_{\text{GRB}}(E)} \tag{5.35}$$

The effective efficiency factor can be applied in the further simulation to each GRB using equation 5.28.

Both methods of determining ε^* agree in the order of 1%. The disagreement could result from a random extra bright GRB in the sample used in the Monte Carlo based method and / or the calculation precision set for the semi-analytic approach.

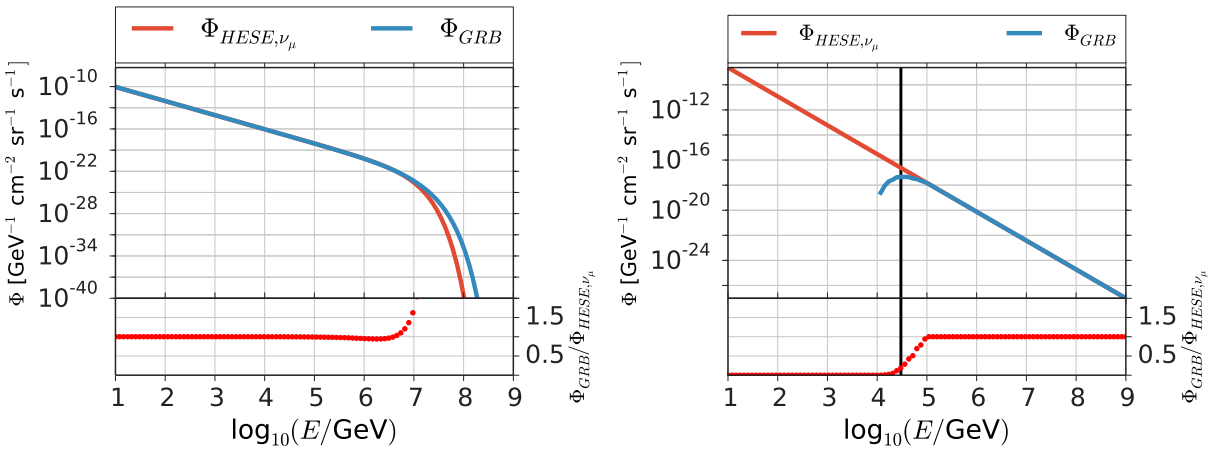

(a) $\hat{E}_{min}$ was set to 1.

(b) $\hat{E}_{min}$ was set to 100 TeV.

Figure 9: Upper plot: The differential flux in energy for the HESE spectrum (E^{-2} with cut-off on the left and $E^{-2/3}$ on the right) and the spectrum produced by all GRBs up to a redshift of 8. Lower plot: ratio between the GRB flux and the HESE flux. The ratio should be equal to one.

5.5.3 Influence of $\hat{E}_{min}$

The influence of the minimal neutrino energy from a GRB has two effects.

The constant Υ in eq. 5.27 becomes smaller the more stringent the energy cut is (Eq. 5.15) leading to a smaller efficiency factor ε as the flux at each energy needs to reproduce the HESE flux. The effective efficiency factor ε^* will stay the same. Using the example of $\hat{E}_{min} = 100$ TeV shown in figure 9b, $\varepsilon^* = 0.92$ was chosen to reach an agreement for as large an energy range as possible.

The other effect can be seen at low energies at which the GRB flux drops to zero. No events with energies

$$E_\nu \leq \frac{\hat{E}_{min}}{1+z} \tag{5.36}$$

can exist in the detector if a minimal neutrino energy cut at source is applied. The GRB flux transitions from an agreement with the HESE flux towards no flux at all because the cut effects are redshift dependent. Neutrinos with higher energies are more effected the closer to earth a GRB is assumed to be. The value $\hat{E}_{min}$ was chosen to create a cut-off at earth at low energies reproducing approximately the lowest measured energy of an HESE event of 30 TeV (black line).

In summary, the effect of a different $\hat{E}_{min}$ on the final flux per energy is non existent. However, events will be lost at lower energies.

5.6 Detection Probabilities

At this stage, the drawing of GRB properties according to the specified functions and the subsequent derivation and calculation of the signal expectation in IceCube has been explained. However, the Optical (and X-ray) Follow-Up does not trigger on singlets but on multiplets fulfilling several criteria.

Multiplets are a number of neutrinos that arrive within 100 s and 3.5 degrees of each other (chapter 2.1). A test statistic was implemented to select the most signal like doublets to trigger Swift Follow-Up observations. Once triggered there is a chance that a source will not be within the FoV of the XRT. The probabilities for two neutrinos to pass these criteria will be explained in this section.

5.6.1 Doublet Probabilities

5.6.1.1 Probability to detect two neutrinos $P_{2\nu}$

In section 5.4.4, the number of expected neutrinos per GRB μ was calculated. Given this number, the probability to see N neutrinos is given with the Poisson distribution

$$P_{\text{Poisson}}(N,\mu) = \frac{\mu^N}{N!}\exp^{-\mu} \tag{5.37}$$

Hence, the probability to see exactly one neutrino and one or more neutrinos is

$$P_{1\nu} = P_{\text{Poisson}}(1,\mu) \tag{5.38}$$

$$P_{\geq 1\nu} = 1 - P_{\text{Poisson}}(0,\mu) \tag{5.39}$$

The subsequent probabilities apply to the case of exactly two detected neutrinos.

$$P_{2\nu} = P_{\text{Poisson}}(2,\mu) = \frac{\mu^2}{2!}\exp^{-\mu} \tag{5.40}$$

5.6.1.2 $P_{\Delta t}$

$P_{\Delta t}$ is the probability that two neutrinos arrive within 100 seconds, the time window specified in the doublet search. It decreases exponentially with time if the lightcurve is assumed to be fast rising with an exponential decay (FRED)

$$P(\Delta t) = 1 - e^{\left(-\frac{\Delta t}{\tau}\right)}. \tag{5.41}$$

τ can be determined according to equation 5.12 given a specific t_{90} (drawn according to 4.7 and converted in agreement with 4.8). For the Optical Follow-Up $\Delta t_{max} = 100$ s is currently set. The effects of different time windows could be examined by choosing different values. However, this is not the focus of this work.

5.6.1.3 $P_{3.5^\circ}$

The second requirement for each neutrino pair is that they arrive with a maximum angular separation of 3.5 degrees. To calculate this probability $P_{3.5^\circ}$ for a given GRB, NuGen events need to be selected from within the zenith band (chapter 5.3.1) and shifted to the GRB direction (chapter 5.4). To save on computation time, 4000 of the NuGen events are selected randomly and the angular differences of the shifted reconstructed directions are determined for each event combination. The probability is then the ratio between the sum of the weight products (term i and j in Eq. 5.27) of all event pairs passing the 3.5° cut and all evaluated pairs

$$P_{3.5^\circ} = \frac{\sum_i \sum_{j=i+1} w_i \cdot w_j | \Delta\Psi(i,j) \leq 3.5^\circ}{\sum_i \sum_{j=i+1} w_i \cdot w_j} \tag{5.42}$$

Though selecting 4000 events randomly speeds up this calculation, combining each event of the selection with all others requires computational power and time. If all events from within the zenith bands were to be considered, all events and therefore the probability $P_{3.5^\circ}$ should be the same for all GRBs coming from the exact same zenith angle suggesting that a parameterization in dependence of the drawn GRB zenith angle should be possible.

About 8000 GRBs are drawn for each season and HESE spectra and the probability calculated according to 5.42. The resulting parameterization $P_{3.5^\circ}(\theta_{\mathrm{GRB}})$ is then used to simulate GRBs in greater numbers. Exemplary, two cases are shown here to demonstrate the quality and the different behavior of the parameterization in different seasons.

The probabilities follow different behaviors in different zenith ranges. Using a hard spectrum with $\gamma = 2$ and the NuGen dataset of the BDT season, the probability is displayed vs θ_{GRB} in a 2d histogram in Fig. 10a. A mean probability value is calculated for each θ_{GRB} bin. The probability follows two different functional behaviors. A hyperbolic tangent is fitted to the data near the pole ($\cos(\theta_{\mathrm{GRB}}) \leq -0.81$)

$$P = a \cdot \tanh(b \cdot (\cos(\theta_{\mathrm{GRB}} - c)) + d \tag{5.43}$$

while a simple polynomial function of the fifth order is used in the second region

$$P = a \cdot \cos^5 \theta_{\mathrm{GRB}} + b \cdot \cos^4 \theta_{\mathrm{GRB}} + c \cdot \cos^3 \theta_{\mathrm{GRB}} + d \cdot \cos^2 \theta_{\mathrm{GRB}} + e \cdot \cos \theta_{\mathrm{GRB}} + f \tag{5.44}$$

Next to the mean probability of each bin, the fits use the coordinates of the mean of these averaged values between the last bin of the first region and the first bin of the last region and the splitting zenith value as an additional data point. The quality of the parameterization was examined by creating a second dataset of GRBs. The probability was calculated according to Eq. 5.42 based on all NuGen events within a zenith region around a GRB ($P^{\mathrm{MC}}_{3.5^\circ}$) and parametrized according to the fit to the first dataset ($P^{\mathrm{param}}_{3.5^\circ}$). A good agreement between the two procedures is presented in Fig. 10b with a maximum deviation of about 1%.

The second example (IC86-2) demonstrates the difference between the IC86-1/2 seasons and the BDT season. The dependence of the zenith angle shows more structure (Fig 11a) and the parameterization is split into four regions. The data in the first one starting at the pole is fitted with a hyperbolic tangent

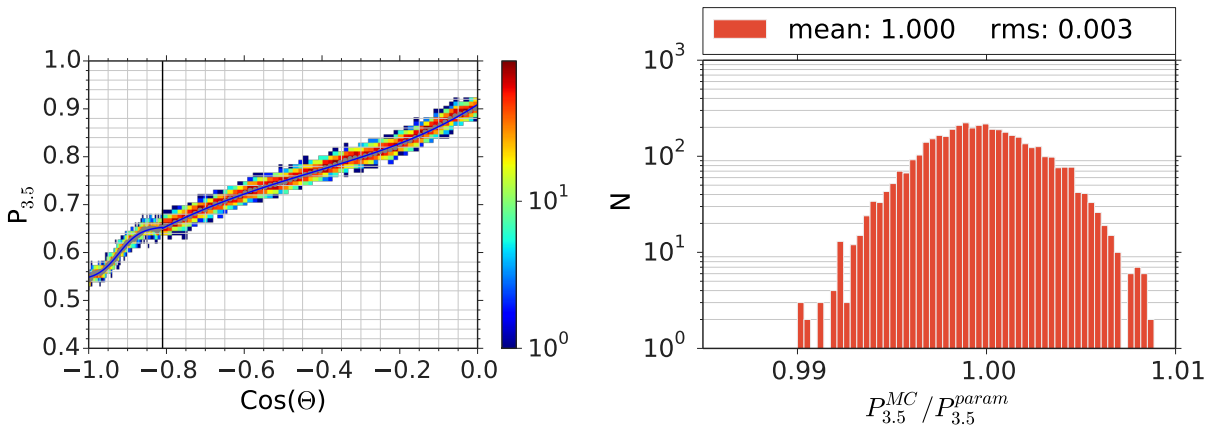

(a) Parametrization (blue line) of the probability $P_{3.5^\circ}$ (b) Testing the parameterization with a second dataset.

Figure 10: IC86-BDT season: The probability of neutrino events to be within 3.5% of each other and the dependency on the cosinus of the GRB zenith angle. The blue line represents the parameterization (left). Using a second set of simulated GRBs, a histogram of the ratio between the calculated probabilities based on all events in the zenith bands and the parametrized values is shown (right). The maximum deviation is about 1%.

(Eq. 5.43) while the data in the other three regions are all fitted with the polynomial function (Eq. 5.44) each.

The quality of the parameterization can be examined in Fig. 11b. The overall result is still very satisfying though the root mean square is with 0.01 instead of 0.003 larger as is the maximum deviation of about 4% instead of 1%. However, the probabilities $P_{3.5^\circ}^{\mathrm{MC}}$ in the second control dataset are not based on all events within the zenith region in this test. Instead, a random selection of 4000 events was used as well leading to possible fluctuations of the comparison points compared to the optimal value based on all events. Thus, the slightly worse but still good result is explained and the parameterization will be used.

The final probability per zenith direction is not dependent on the absolute normalization of the flux as it cancels in equation 5.42, but on the chosen OFU cuts and the spectral shape. The season and the signal spectrum define the amount events of different energies contribute to the calculation. Therefore, the probability is parametrized once per season and spectral index γ and is then used for all GRB models. The root-mean-square suffers by about 0.1 - 0.2 percentage points in comparison to individual parameterizations per season, γ and GRB model and is considered acceptable.

The fitted values to the free parameters in Eq. 5.43 and 5.44 as well as the break points between the different regions are listed for all season - spectra combinations in table 6.

5.6.1.4 Doublet Probability

The probability that two neutrinos coincide as a doublet that triggers OFU is then

$$P_{\mathrm{D}} = P_{\Delta t} \cdot P_{3.5^\circ} \tag{5.45}$$

5.6.1.5 $\mathrm{P_{llh}}$

On average the doublet selection based on time and direction leads to about 50 - 60 doublets per year (depending on season) while only seven alerts can be sent to the Swift telescope. The selection of the most signal like doublets is based on the OFU test statistic 2.3.

The test statistic is calculated for all event pairs that pass the condition of being reconstructed within 3.5° (denoted as $\mid \Delta\Psi(i,j) \leq 3.5^\circ$). They are given a total weight by multiplying the individual event weights. The time difference is randomly drawn with $\Delta T \in [0, 100]$ s and weighted according to an exponential decay

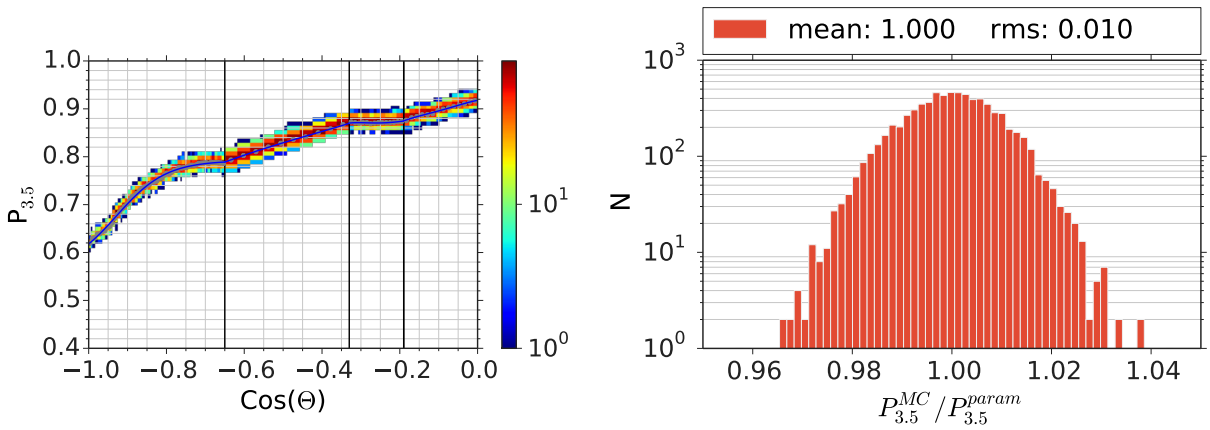

(a) Parametrization (blue line) of the probability $P_{3.5^\circ}$ (b) Testing the parameterization with a second dataset.

Figure 11: IC86-2 season: The probability of neutrino events to be within 3.5% of each other and the dependency on the cosinus of the GRB zenith angle. The blue line represents the parameterization (left). Using a second set of simulated GRBs, a histogram of the ratio between the calculated probabilities based on all events in the zenith bands and the parametrized values is shown (right). The maximum deviation is about 4%.

(Eq. 5.9) introducing a dependency on t_{90} (Eq. 5.12). The probability that a GRB doublet will pass the cut λ_{cut} is determined by taking the ratio of the weight sum of doublets passing λ_{cut} and the weight sum of all considered doublets.

$$P_{\text{llh}} = \frac{\sum_i \sum_{j=i+1} w_i \cdot w_j \mid \lambda(i,j) \leq \lambda_{\text{cut}} \mid \Delta\Psi(i,j) \leq 3.5^\circ}{\sum_i \sum_{j=i+1} w_i \cdot w_j \mid \Delta\Psi(i,j) \leq 3.5^\circ} \tag{5.46}$$

The parameterization of P_{llh} is more complicated than $P_{3.5^\circ}$. The test statistic depends not only on properties of the simulated neutrino events like the zenith angle but on the time window between two neutrinos and, therefore, on t_{90}. The data is split into 180 cosinus bins and the probability is fitted against the logarithm of the drawn t_{90} (Eq. 4.7 and 4.8) value for each bin. The amount of 180 bins is a compromise between precision and needed computational power. The probability changes rapidly near the pole requiring a high number of bins. In return, many simulated GRBs are needed to facilitate a good parameterization representing various GRBs per bin and t_{90} value.

An example based on a dataset for the IC86-BDT season and a spectral index of $\gamma = 2$ is shown in Figure 12 displaying individual calculated probabilities of GRBs as red dots and a fit to these points as a function of the logarithm of t_{90}. The fit is based on Eq. 5.43. Such a fit is done for each bin in $\cos\theta_{\text{GRB}}$ and for each season - γ combination in turn. Due to the large number of plots only an example is displayed.

The quality of the parameterization can be judged by examining Figure 13a. The parameterization was applied to a second dataset for which the probability was calculated according to 5.46 for all events within the zenith band. The ratio of calculated and parametrized values are displayed in the histogram. Both the root mean square with 0.006 and the maximum deviation with about 3 percentage points are satisfactory small.

5.6.1.6 P_{onS}

The Optical Follow-Up program calculates the weighted mean direction from all events contributing to a multiplet using the Cramer Rao error as weights. For a source to be detectable with Swift, its direction must be within 0.5 degrees of the true source direction. The probability P_{onS} for two events to point back to the source well enough is given by the ratio of the sum over the event weight products fulfilling the condition

season	γ	region	b_i	a	b	c	d	e	f
IC86-1	2	I	-1	0.113	7.847	-0.923	0.680	-	-
IC86-1	2	II	-0.65	1.206	2.472	7.126	9.782	4.855	
IC86-1	2	III	-0.33	3.257e-02	-1.455e+01	-9.1460e+01	-2.488e+02	-2.481e+02	
IC86-1	2	IV	-0.21	9.198e-01	3.415e-02	-3.649e+00	-2.404e+01	-5.053e+01	
IC86-2	2	I	-1	0.115	7.857	-0.928	0.678	-	-
IC86-2	2	II	-0.65	1.041	0.910	2.191	2.687	1.140	
IC86-2	2	III	-0.33	0.753	-2.582	-18.718	-56.052	-59.955	
IC86-2	2	IV	-0.19	0.918	0.156	-1.679	-14.0167	-37.505	
IC86-BDT	2	I	-1	0.056	17.705	-0.923	0.598	-	-
IC86-BDT	2	II	-0.81	0.909	0.525	0.728	0.724	0.171	
IC86-1	2.3	I	-1	0.121	8.142	-0.915	0.649	-	-
IC86-1	2.3	II	-0.66	0.699	-1.484	-4.571	-5.137	-2.116	
IC86-1	2.3	III	-0.33	0.463	-7.566	-51.675	-149.622	-156.750	
IC86-1	2.3	IV	-0.22	0.907	0.149	-1.409	-6.671	-9.912	
IC86-2	2.3	I	-1	0.127	7.667	-0.924	0.640	-	-
IC86-2	2.3	II	-0.66	0.843	-0.357	-1.481	-1.560	-0.640	
IC86-2	2.3	III	-0.33	2.351e-02	-1.387e+01	-8.545e+01	-2.300e+02	-2.273e+02	
IC86-2	2.3	IV	-0.21	0.904	0.169	-1.130	-2.400	5.261	
IC86-BDT	2.3	I	-1	0.066	18.423	-0.925	0.560		
IC86-BDT	2.3	II	-0.81	0.899	0.638	1.153	1.339	0.454	
IC86-1	2.7	I	-1	0.130	8.742	-0.906	0.592	-	-
IC86-1	2.7	II	-0.65	-0.448	-10.910	-33.936	-44.693	-21.645	
IC86-1	2.7	III	-0.32	19.454	276.583	1531.855	3754.553	3435.745	
IC86-1	2.7	IV	-0.23	0.873	0.077	-2.717	-9.764	-7.907	
IC86-2	2.7	I	-1	0.150	7.004	-0.922	0.573	-	-
IC86-2	2.7	II	-0.66	0.430	-3.295	-9.984	-12.148	-5.474	
IC86-2	2.7	III	-0.33	1.965	15.083	71.629	147.549	111.037	
IC86-2	2.7	IV	-0.22	0.872	0.236	-0.210	14.100	61.454	
IC86-BDT	2.7	I	-1	0.079	18.777	-0.929	0.489	-	-
IC86-BDT	2.7	II	-0.81	0.874	0.919	2.247	2.942	1.226	

Table 6: The fit values to the parameters in functions 5.43 and 5.44. e and f are marked '-' if the first function was used. All values have been rounded to the third decimal place. The break points b_i denote the left starting point of a region in $\cos\theta_{\mathrm{GRB}}$.

and the sum over all event weight products:

$$P_{\mathrm{onS}} = \frac{\sum_i \sum_{j=i+1} w_i \cdot w_j | \Psi_{\text{weighted mean}}(i,j) - \Psi_{GRB} \leq 0.5^\circ \mid \lambda(i,j) \leq \lambda_{\mathrm{cut}} \mid \Delta\Psi(i,j) \leq 3.5^\circ}{\sum_i \sum_{j=i+1} w_i \cdot w_j \mid \lambda(i,j) \leq \lambda_{\mathrm{cut}} \mid \Delta\Psi(i,j) \leq 3.5^\circ} \tag{5.47}$$

Only events passing the conditions $\Delta\Psi(i,j) \leq 3.5^\circ$ and $\lambda(i,j) \leq \lambda_{\mathrm{cut}}$ are considered. The parametrization is performed using the methods used and described for P_{llh} leading to a similar quality as can be judged with the help of Figure 13b.

5.6.1.7 Alert Probability

The probabilities described in this section until now are conditional and can be combined via multiplication according to the Base Theorem and the probability that two neutrinos are detected, trigger the Swift Follow-Up and that the source is within Swifts FoV is

$$P_{\mathrm{Alert}} = P_{2\nu} \cdot P_D \cdot P_{\mathrm{llh}} \cdot P_{\mathrm{onS}}. \tag{5.48}$$

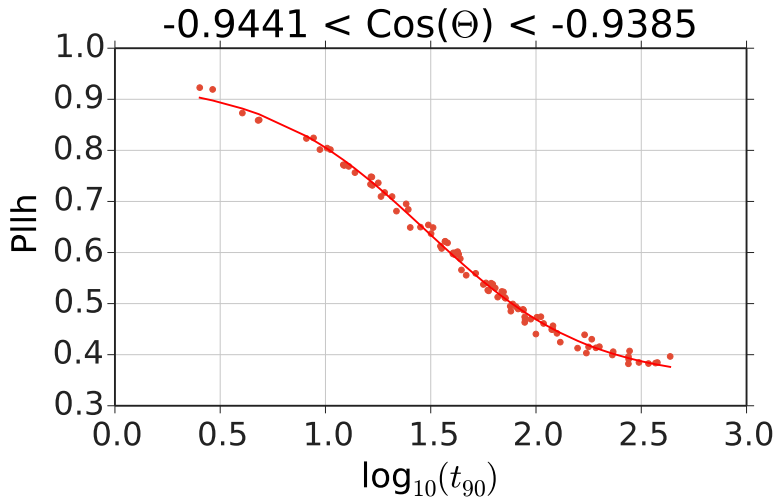

Figure 12: The probability for a doublet to pass the cut on the likelihood (Eq. 2.3) vs the logarithm of t_{90}. As an example, the cosinus bin of $-0.9441 < \cos\theta_{\mathrm{GRB}} < -0.9385$ is shown. The red dots represent values calculated according to Eq. 5.46 for drawn GRBs. The red line is a fit to these values.

P_{onS} can be set to one if only the probability to have a Swift alert is of interest.

Given these parameterizations, a big number of usually around five million GRBs are thrown to create a sample representing the complete redshift and luminosity range.

5.6.2 Probability to Detect a GRB

The previous section described a simplified case of only two neutrinos. However, if μ neutrinos are expected per GRB there is a chance to see more than two neutrinos. There are two trigger conditions for a Swift alert. Usually, one doublet is detected and passes the Swift cut on the OFU test statistic as well. However, there is the possibility of a 'higher multiplet' as well which we define as an alert of at least three neutrinos.

In both cases the number of possible doublets and the probability of them to be detected needs to be calculated. If N neutrinos are detected, the first neutrino can be part of a doublet with $N-1$ partners, while the second neutrino can combine with $N-2$ partners. The general formula describing the number of possible combinations is the Gaussian Sum Formula

$$d = 1+2+\ldots+(x-1)+x = \frac{x^2+x}{2}. \tag{5.49}$$

Two neutrinos are needed to form a doublet, leading to the substitution $N = x-1$. The number of possible doublets is then

$$d = \frac{N^2-N}{2}. \tag{5.50}$$

with each doublet having a probability P_D to pass the time window and angular separation cuts. The probability for this to happen k out of d times is given by the binomial distribution

$$P_{\mathrm{bin}}(k,d(N),P_D) = \binom{d}{k}\cdot P_D^k\cdot(1-P_D)^{d-k} = \binom{0.5(N^2-N)}{k}\cdot P_D^k\cdot(1-P_D)^{0.5(N^2-N)-k} \tag{5.51}$$

The correct probability to see exactly one doublet to is determined by multiplying the probability to see N neutrinos and the probability of these N neutrinos to form exactly one doublet for all $N \geq 2$

$$P_{1\ \mathrm{Doublet}} = \sum_{N=2}^{N_{\mathrm{max}}} P_{\mathrm{Poisson}}(N,\mu)\cdot P_{\mathrm{bin}}(1,d(N),P_D) \tag{5.52}$$

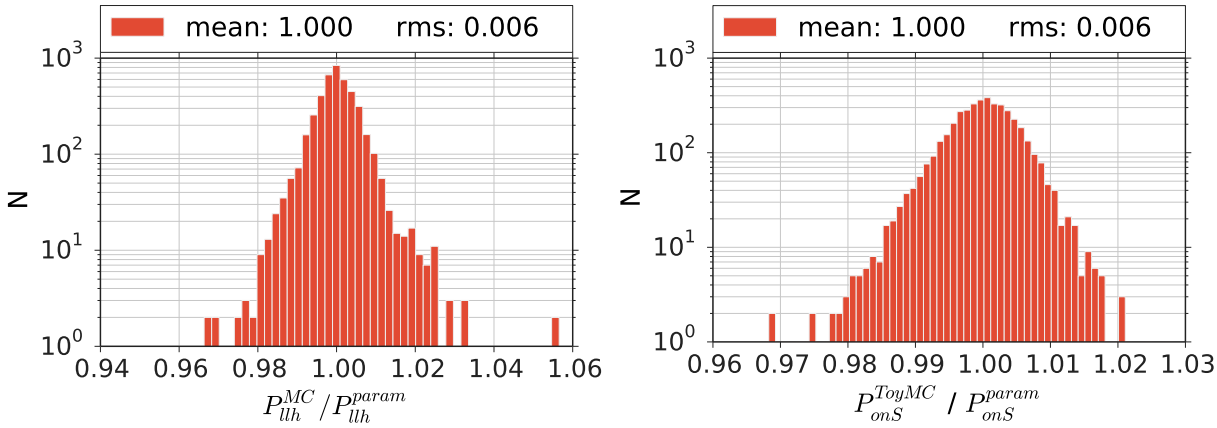

(a) Probability to pass likelihood cut.

(b) Probability for a GRB to be within Swift FoV.

Figure 13: Season IC86-BDT: Using a second set of simulated GRBs, a histogram of the ratio between the calculated probabilities and the parametrized values is shown. The maximum deviation is of about 2 percentage points.

N_{max} is chosen to achieve a precision in the order of 10^{-6}. The probability that one doublet passes the likelihood cut as well is given by

$$P_{\text{1 Swift Doublet}} = P_{\text{1 Doublet}} \cdot P_{\text{llh}} \tag{5.53}$$

The second channel is triggered when at least three neutrinos result in at least two doublets.

$$P_{\text{Multiplet}} = \sum_{n=3}^{n_{\text{max}}} P_{\text{Poisson}}(n,\mu) \cdot [1 - P_{\text{bin}}(0, d(n), P_D) - P_{\text{bin}}(1, d(n), P_D)] \tag{5.54}$$

These definitions can be used to calculate the probability to detect a specific GRB. Generating $N_{\text{gen}} = 5 \cdot 10^6$ GRBs, the number of GRBs that are expected to be detected in a specific channel is the sum over all probabilities, e.g. for higher multiplets

$$N_{\text{GRB}}/yr = \sum_{i=0}^{N_{\text{gen}}} P_{\text{multiplet},i} \cdot \frac{N_{\text{GRB, yr}}}{N_{\text{GRB, gen}}} \tag{5.55}$$

The ratio at the end is necessary to renormalize the result to the expected number of GRBs per year $N_{\text{GRB, yr}}$.

This concludes the description of the Toy Monte Carlo to calculate the expected number of expected signal alerts for different spectra and GRB models. The following section describes how to use the background and signal expectations to calculate a test statistic. It will be used to draw limits on the contribution of transients to the HESE flux.

6 Significance and Limit calculation

This section will describe the test statistic to evaluate the conformity with background of the measured alerts. The test statistic is based on multiplying the p-values of different components which can be separated into two categories: the pure number of alerts and the probability that doublets stem from background.

The Optical Follow-Up was designed with the expectation that most of the alerts will be triggered due to background events of atmospheric neutrinos. An excess of detected multiplets in comparison to the expected background average can indicate a possible signal contribution.

Given the average background expectation $\mu_{k,b}$ for multiplets with multiplicity k (Table 4), the probability to see N_k or more alerts during one season is

$$P(N_k, \mu_k) = \sum P_{\text{Poisson}} = \sum_{i=N_k}^{\infty} \frac{\mu_k^i}{i!} \exp^{-\mu_k}. \tag{6.1}$$

The sum is aborted when a precision of 10^{-6} is reached. The probabilities for the different multiplicities k and seasons i are then multiplied to form the test statistic λ_{na} to evaluate the number of alerts

$$\lambda_{na}\left(N_k^i, \mu_{k,b}^i\right) = \prod_{k=2}^{\infty} \prod_i P(N_k^i, \mu_{k,b}^i). \tag{6.2}$$

The second component is only valid for doublets as higher multiplicities are automatically considered true alerts. The OFU system generates up to about 50 doublets per year of which only seven can be sent to Swift. The down selection is based on the OFU test statistic (Eq. 2.3) separating the more signal like and the more background like doublets. For each doublet an OFU test statistic value is drawn and compared to the background distribution to calculate the p-value $p_{j,i}^{ofu}$. The p-values of all doublets can not simply be multiplied as the number of doublets would influence the significance of the test statistic. E.g. three background doublets would form a smaller overall p-value $O(10^{-3})$ than one signal doublet $O(10^{-1})$. A combination of all $p_{j,i}^{ofu}$ was chosen to keep the total contribution in the same order of magnitude independent of the number of doublets. The geometric mean is calculated of all $p_{j,i}^{ofu}$ with N_2^i being the number of considered doublets of season i

$$\lambda_{\text{ofu}} = \prod_i \sqrt[N_2^i]{\prod_{j=1}^{N_2^i} p_{j,i}^{ofu}} \tag{6.3}$$

Calculating $p_{j,i}^{ofu}$ is based on several steps. The OFU test statistic distribution differs slightly for different zenith regions. To evaluate the correct test statistic a zenith value is drawn for each doublet according to the the correct cosinus distribution for Swift doublets. For background, these distributions are generated for each season when scrambling the data (Fig 14a). The signal distributions are highly dependent on signal strength and spectrum shape as high energy neutrinos are less likely to pass through the earth. Therefore, a distribution is generated for each season - spectrum - signal strength combination. One example can be seen in Figure 14b.

The northern sky was divided into twenty even regions in $\cos(\theta)$ and the probability density functions of the OFU test statistic were created for background and signal of all considered spectra for all seasons in each region. An example is shown in Figure 15a for the first zone from the pole for the IC86-BDT season. Using the zenith value the correct OFU test statistic probability density function is chosen to draw a test statistic value. As the probability to have a Swift doublet is already included in calculating the expected number of doublets μ_2^i, the test statistic value must be smaller than the Swift cut of the season. The chosen value is then compared to the cumulative background distribution (Figure 15b) and the p-value is extracted.

The complete test statistic is the combination of both components

$$\lambda = \lambda_{na} \cdot \lambda_{\text{ofu}} \tag{6.4}$$

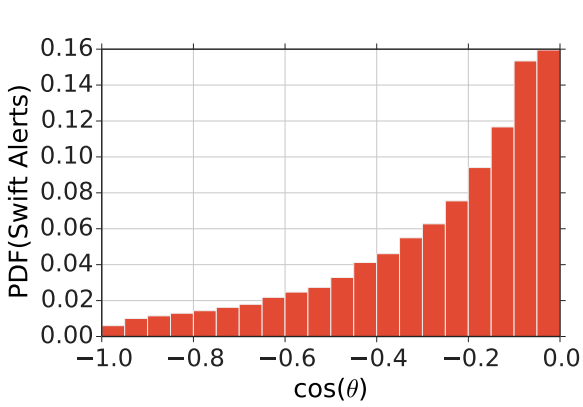

(a) Background distribution for IC86-BDT

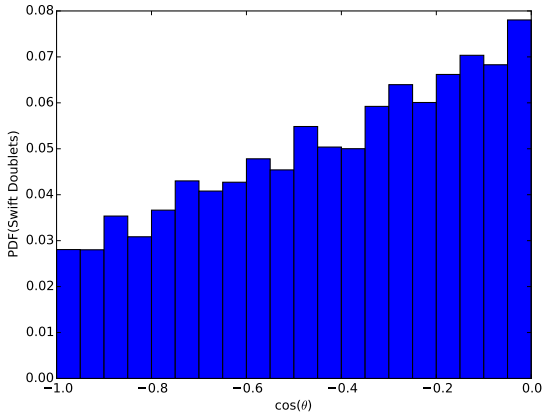

(b) Signal distribution for IC86-BDT

Figure 14: The plots show the cosinus zenith distribution of Swift doublets for background of the IC86-BDT season and for a signal distribution of the BDT season with a spectrum with $\gamma = 2.3$ and one specific signal expectation.

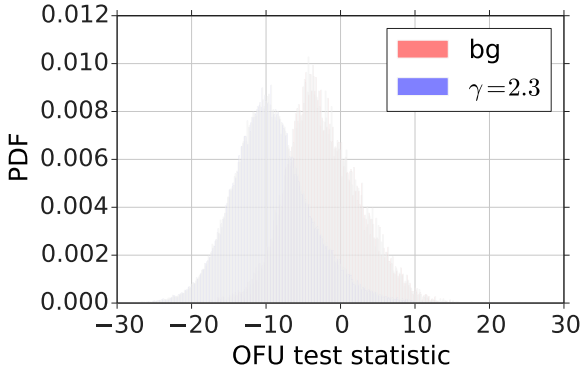

(a) The probability density functions

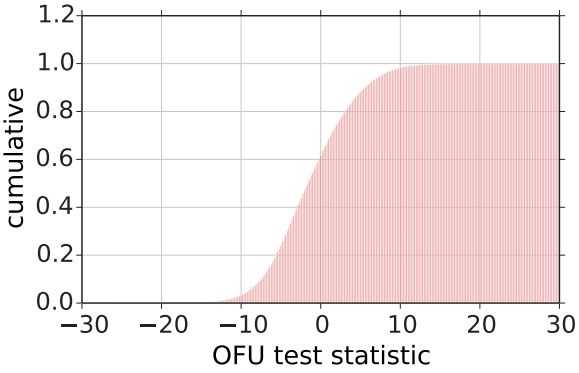

(b) Cumulative distribution of background .

Figure 15: The OFU test statistic (background and signal with a spectral index of $\gamma = 2.3$) for the first region starting from the pole for the IC86-BDT season.

The final significance and limit calculation is based on running pseudo experiments. To evaluate the agreement of the measured alerts with a pure background hypothesis, the average background expectation $\mu^i_{k,b}$ per season i and multiplicity k is used to draw a number of detected multiplets N^i_k according to a Poisson distribution. For all N^i_2 doublets, $p^{ofu}_{j,i}$ is calculated. In total, 10^6 experiments are performed per season and the resulting test statistic values are compared to the measured result (λ_m). The p-value is the fraction of experiments with worse agreement to the background hypothesis ($\lambda < \lambda_m$).

Similarly, a signal hypothesis can be tested. The GRB Toy Monte Carlo is used to estimate the average number of expected multiplets $\mu^i_{k,s,\gamma}$ for a specific model and $N^i_{k,s,\gamma}$ values are again generated according to the Poisson distribution. The number of alerts $N^i_{k,s+b}$ is the combination of background and signal alerts

$$N^i_{k,s+b} = N^i_{k,s} + N^i_{k,b}. \tag{6.5}$$

The influence of the OFU test statistic (Eq. 6.3) is

$$\lambda_{\text{ofu}} = \prod_i \sqrt[N^i_{2,s+b}]{\prod_{j=1}^{N^i_{2,b}} p^{ofu}_{j,i,b} \cdot \prod_{j=1}^{N^i_{2,s}} p^{ofu}_{j,i,s}} \tag{6.6}$$

10^6 experiments are performed per season and GRB model as well and the test statistic (Eq. 6.4) evaluated. A model can be ruled out at 90% confidence level if 90% of the experiments show a worse agreement with the background only hypothesis than the actual experimental results. An example is shown in Figures 16a and 16b.

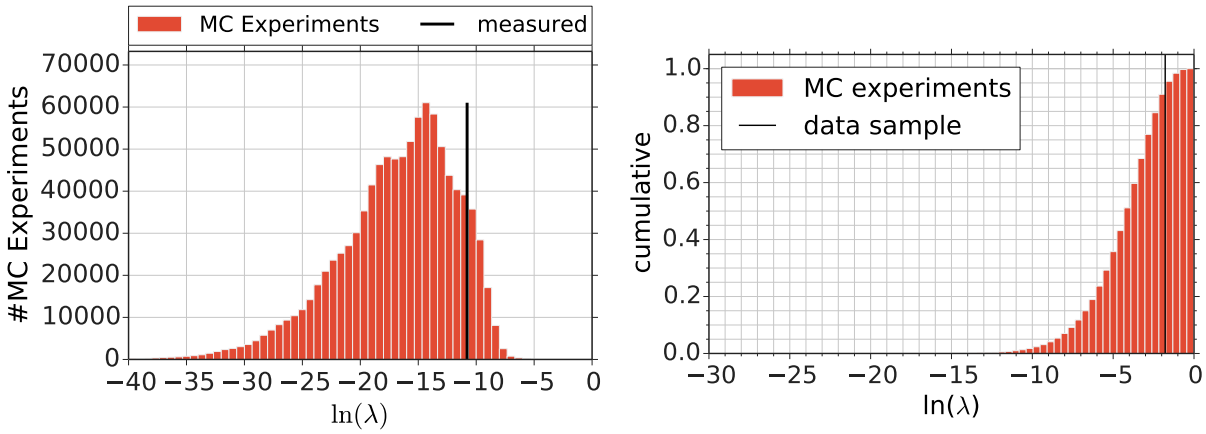

(a) Differential distribution

(b) cumulative distribution

Figure 16: 10^6 experiments were thrown and the test statistic λ was calculated according to equation 6.2. In read is the differential distribution of the Monte Carlo experiments while the black line represents the detected value. About 90% of the experiments have a worse agreement with the background only hypothesis.

7 Results

The whole simulation setup and the methodology described in the last sections can be used to draw limits on the contribution of GRBs and other short transients to the detected diffuse high energy neutrino flux (HESE flux). The results and the impacts of different models is described in this section.

7.1 Limits on Contribution to the HESE Flux by Transient Neutrino Sources

In chapter 6, the methodology to calculate limits on the contribution of a transient population to the HESE flux was described. The pseudo experiments need to be repeated for each different signal model. The result for a spectrum with $\gamma = 2.3$, 3000 GRBs per year and a fraction of 5.95% of the HESE flux to be produced by these GRBs are shown in Figures 16a and 16b. The GRB rate density is not a known value but a parameter. To calculate the p-value for different rate densities and fraction of contribution to the HESE flux, the signal expectation μ_s can be scaled by

$$\hat{\mu}_s = \mu_s \cdot \zeta \frac{3000\text{GRBs/yr}}{N_{\text{GRBs/yr}}} \tag{7.1}$$

with ζ being the contribution to the total HESE flux. By doubling the number of GRBs, the neutrino flux per GRB gets reduced by half, leading to softer limits.

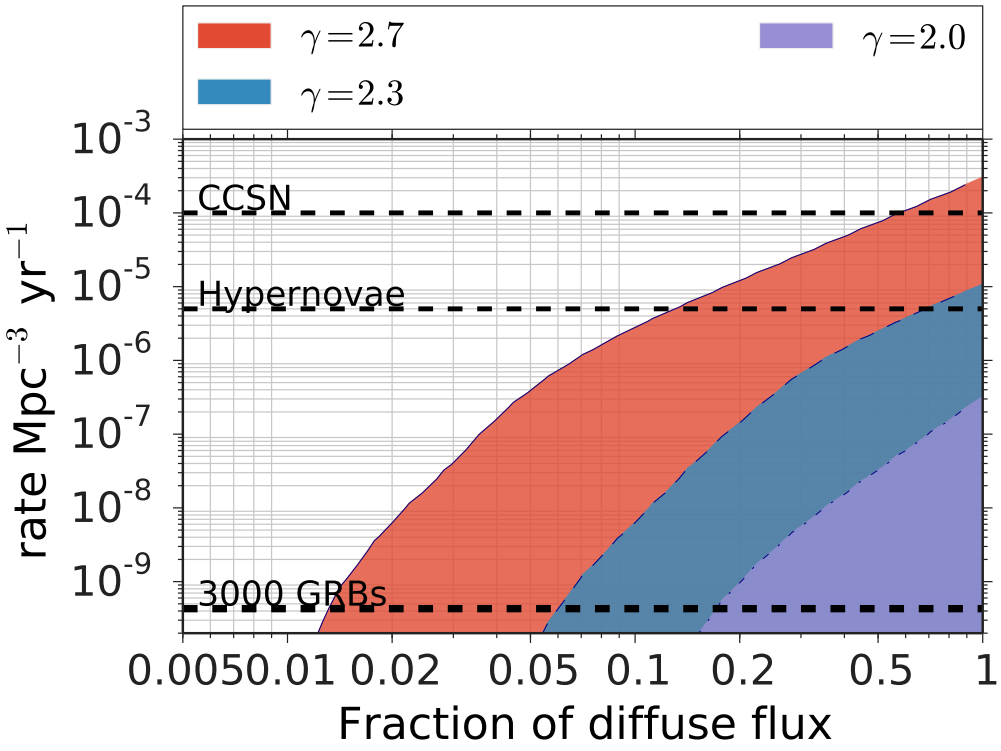

Figure 17: Limits on the contribution of short transient sources to the HESE flux depending on their rate density. The 90% confidence regions are shown for three different spectra using the WP model.

Figure 17 showcases the limits for the three different spectra using the WP model. The softer the spectrum the more singlets are expected especially at lower energies (Fig. 8) increase the multiplet expectation as well. Therefore, the hardest limits can be drawn using a spectrum with $\gamma = 2.7$ decreasing in power the harder the spectrum gets. The results for a flux to be ruled out at a 90% confidence level are listed in Table 7.

γ	$N_{\mathrm{GRB/yr}}$	ζ
2.7	3000	0.013
2.3	3000	0.0595
2.0	3000	0.18

Table 7: The values of the fraction to the HESE flux and the number of GRBs per year that are ruled out at a 90% confidence level.

7.1.1 Signal origin

To answer the question on which GRBs the limits are most reliant on, the dependence on the luminosity and the redshift is examined at the 90% confidence limit point for 3000 GRBs per year. Representing the different season and spectra, the BDT season and the intermediate spectrum with $\gamma = 2.3$ were selected.

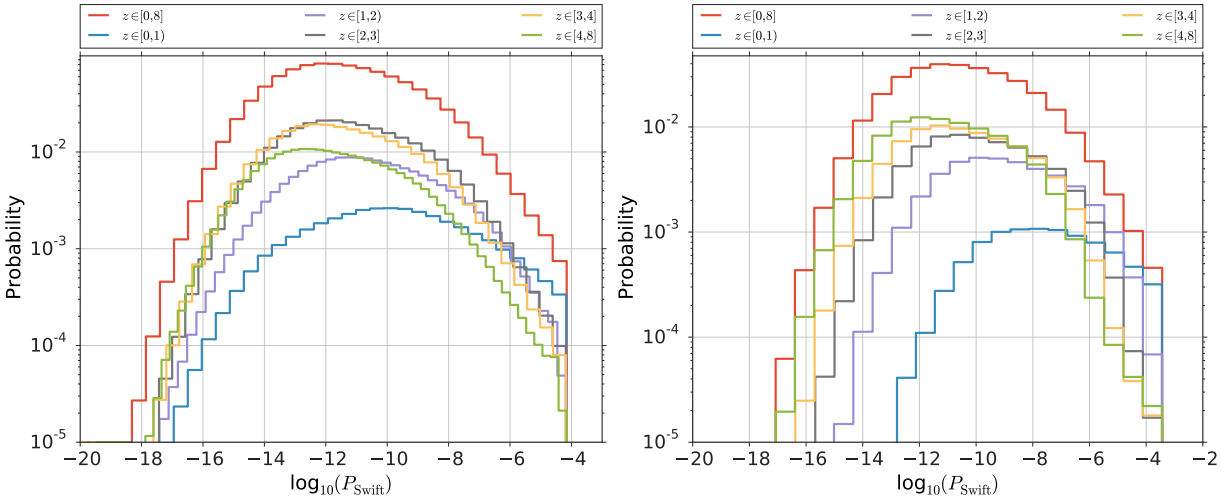

(a) WP model

(b) HC model

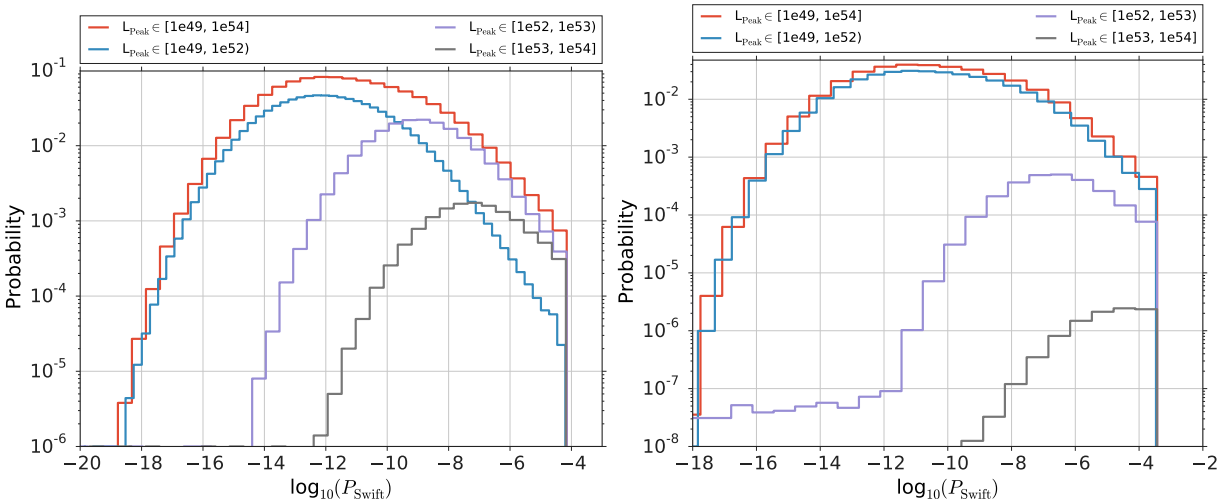

(c) WP model

(d) HC model

Figure 18: The probability for a GRB to have a certain probability to produce a Swift doublet. The contribution of the whole signal and the contribution of various redshift and luminosity bins are shown. Note that contributions with very small probabilities (P_{Swift}) were cut off to display the more relevant region.

In Figure 18a, one can see the probability of a GRB to have a certain probability P_{Swift} for a swift doublet to be detected. Most GRBs are in a redshift range between 2 and 4 which corresponds to the peak in the redshift distribution in Figure 3b. However, these GRBs and the GRBs further out mostly contribute to the

distribution for low to intermediate P_{Swift} values. The most likely GRBs to be seen in IceCube with high P_{Swift} values are within a redshift of one even though they occur less frequent due to the small volume. In total, about 0.3 GRBs per year are expected to be detectable with Swift doublets within the BDT season. About 35% of which would be within the first redshift bin (Figure 19a). However, the other regions all contribute more than 10% to the total signal as well.

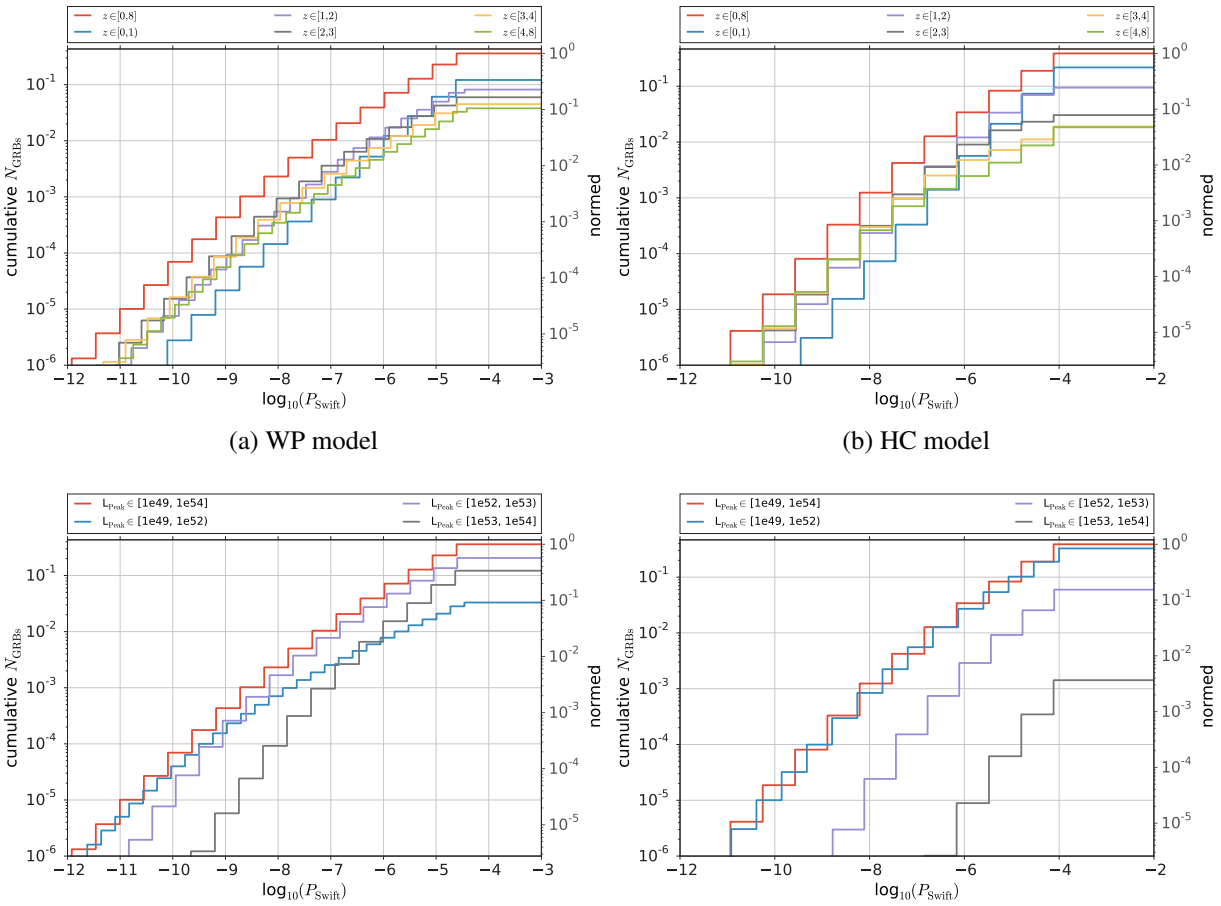

(a) WP model (b) HC model

(c) WP model (d) HC model

Figure 19: The cumulative distribution to the number of GRBs detected per year depending on the probability to produce a Swift doublet. The contribution of the whole signal and the contribution of various redshift and luminosity bins are shown. On the right y-axis, the values are divided by the complete number of GRBs produced per year, thus, showing the fraction contributed by the different bins. Note that contributions with very small probabilities (P_{Swift}) were cut off to display the more relevant region.

Similar plots can be examined in Figures 18c and 19c examining the influence of the peak luminosity. Low luminosity GRBs of less than 10^{52}erg/s produce mainly GRBs with low detection probability only contributing about 10% to the expected number of detectable GRBs. The main contribution of almost 60% stems from GRBs with peak luminosities within 10^{52} and 10^{53}erg/s by compromising between abundance and brightness. However, this describes the cumulative contribution of all GRBs, the most likely GRBs to be actually detectable are very bright and very close GRBs. Unfortunately, they happen rather seldom.

The same comparison can be done for the probability to see higher multiplets of at least three neutrinos (Figures 20c and 20a). The signal is more dependent on the very bright and close GRBs as others do not produce the necessary flux to make a detection likely. The contribution to the total number of 0.5 detectable GRBs per year with the BDT season setup drops to about 6% for the low luminosity GRBs while the very close GRBs up to a redshift of one constitute about 80% of the total signal for higher multiplets.

Combining these results, one can see that we expect most signal from the very rare and close GRBs within a redshift of one. The number of detectable GRBs per year is displayed over the redshift in Figure 21a. Both

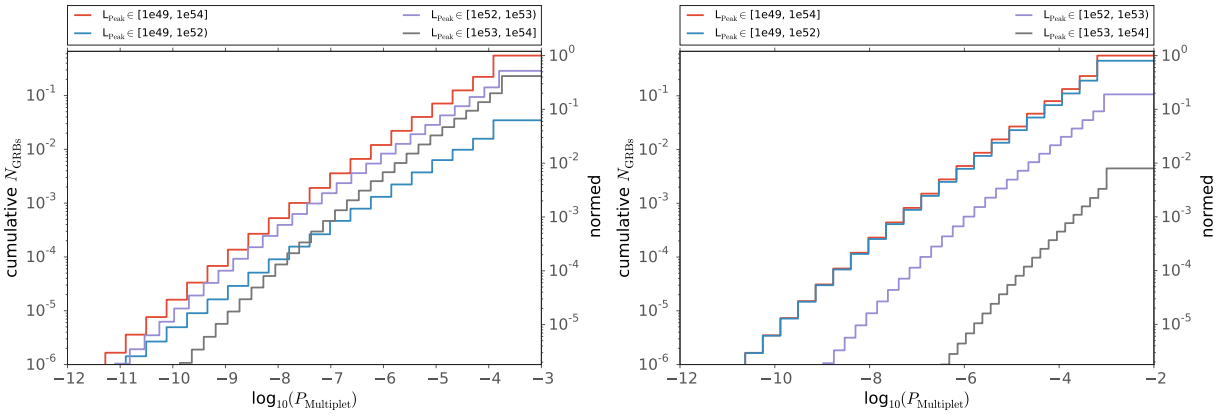

(a) WP model

(b) HC model

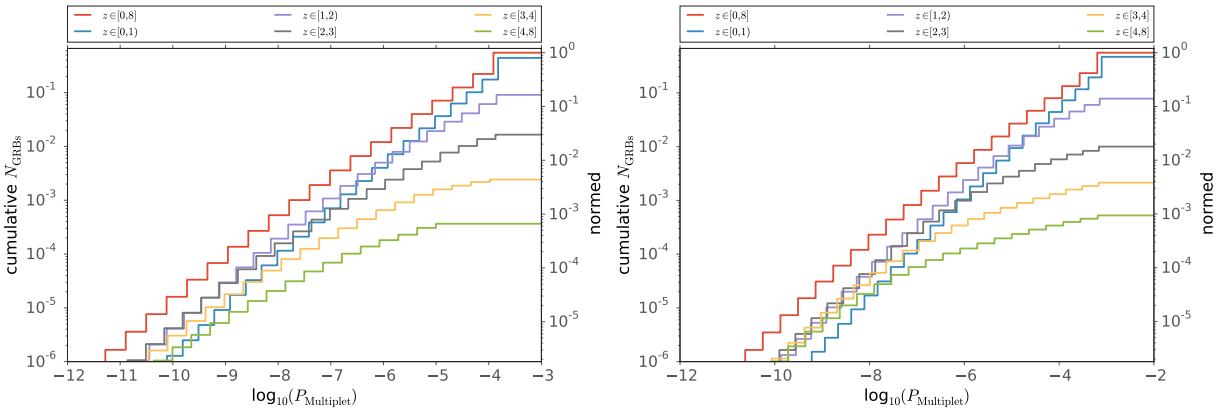

(c) WP model

(d) HC model

Figure 20: The cumulative distribution to the number of GRBs detected per year depending on the probability to produce a higher multiplet. The contribution of the whole signal and the contribution of various luminosity and redshift bins are shown. On the right y-axis, the values are divided by the complete number of GRBs produced per year, thus, showing the fraction contributed by the different bins. Note that contributions with very small probabilities ($P_{\text{Multiplet}}$) were cut off to display the more relevant region.

channels - the detection with swift doublets and higher multiplets - peak in the number of GRBs per year for GRBs within the first redshift bin with the multiplets dominating the signal strength. GRBs at these ranges produce a neutrino flux high enough that it is more likely to see multiplets than swift doublets. Exploring the cosmos to higher redshifts, the flux decreases and starting at about $z = 1$ it is more likely to see swift doublets. However, the chance to be seen at all decreases as well, limiting the contribution to the cumulative signal with anything above $z = 2$ only summing up to about 1% of the combined multiplet and swift doublet signal. Combined with the fact that in contrast to the doublets there is very limited multiplet background, the higher multiplet channel is the main contributer to the 90% confidence point for an expected 3000 GRBs per year.

Reducing the fraction of contribution to the HESE flux by GRBs, reduces the flux per GRB and as such the importance of the multiplet channel as well. A similar effect is to be expected by looking at higher rate densities. With more sources producing the same diffuse neutrino flux, the flux per source decreases.

7.2 Different models

So far, the Wanderman Piran model was examined to present the results of the analysis. The influence of two different factors will be analyzed in the subsequent sections.

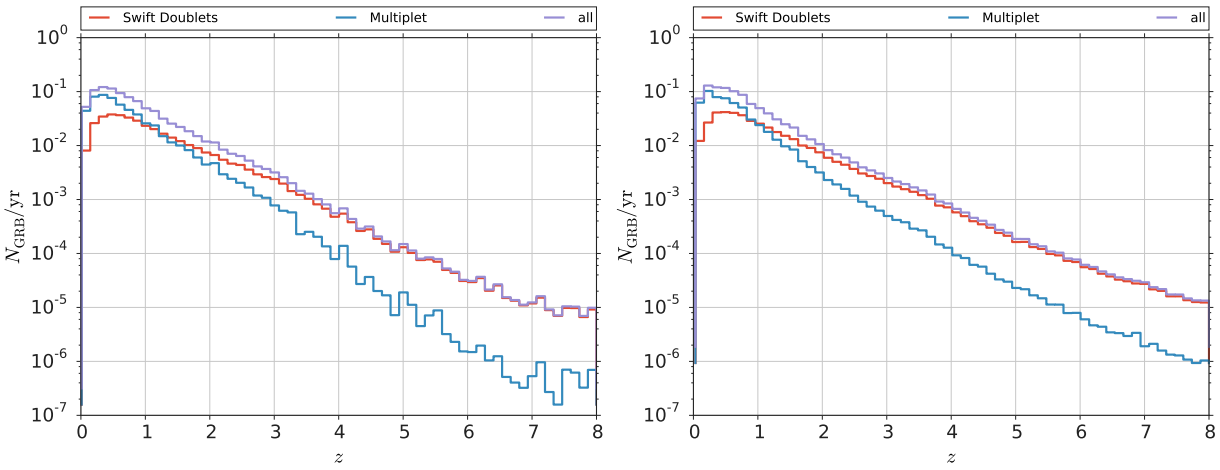

(a) WP model

(b) HC model

Figure 21: The cumulative distribution to the number of GRBs detected per year depending on the probability to produce a higher multiplet. The contribution of the whole signal and the contribution of various luminosity and redshift bins are shown. On the right y-axis, the values are divided by the complete number of GRBs produced per year, thus, showing the fraction contributed by the different bins. Note that contributions with very small probabilities ($P_{\mathrm{Multiplet}}$) were cut off to display the more relevant region.

The WP model is based on a broad luminosity function. The resulting variation in luminosity can lead to seldom but very bright GRBs producing the most detectable signal. Two different luminosity functions will be examined, the Howell Coward model (Section 7.2.1) and a more SN conform luminosity distribution (Section 7.2.2).

The second factor is a low energy cut-off, having great influence on the final limits on the HESE flux contribution (Section 7.2.3).

7.2.1 Howell Coward

The Howell Coward model (Section ???) predicts various luminosity distributions that have one thing in common when compared to WP: less GRBs are predicted at high peak luminosity values (Fig. 5a). While the slope at low peak luminosities is with $\alpha_{WP} = -0.17$ and $\alpha_{HC} = -0.13$ quite similar, the distributions diverge quite strongly above $L_{\mathrm{Peak}} \geq 1e52\mathrm{ergs}^{-1}$ and the HC luminosity function drops with $\beta HC = -2.42$ much faster than the WP function ($\beta WP = -1.44$).

The impact of this deviating behavior will be examined for the flux model with a spectral index of $\gamma = 2.3$ as the intermediate model. The result can be seen in Figure 22 displaying the less stringent limits of the HC model. Assuming 3000 contributing GRBs per year, the contribution to the HESE flux of GRBs following the HC luminosity can be determined at a 90% confidence level to be less than 7.59% (WP: 5.95%). This point will be examined in more detail in the following paragraphs.

Looking at the luminosity distribution (Fig. 5a) already indicates that high luminosity GRBs will have less impact for the HC model than the WP model as they are suppressed in frequency by almost four orders of magnitude at the highest luminosities of $10^{54}\mathrm{erg/s}$ alone. Figure 18d demonstrates that the low luminosity GRBs dominate the whole range of detection probabilities (P_{Swift}) even to the highest values contributing a total of about 90% to the cumulative swift doublet signal (Fig. 19d). The other GRBs mainly occur at high probability values but lack influence nonetheless due to their sparsity.

Not having the abundance of bright GRBs to produce high neutrino fluxes even at great distances, the cumulative swift doublet signal depends with almost 60% on GRBs within a redshift of one (WP: 35%).

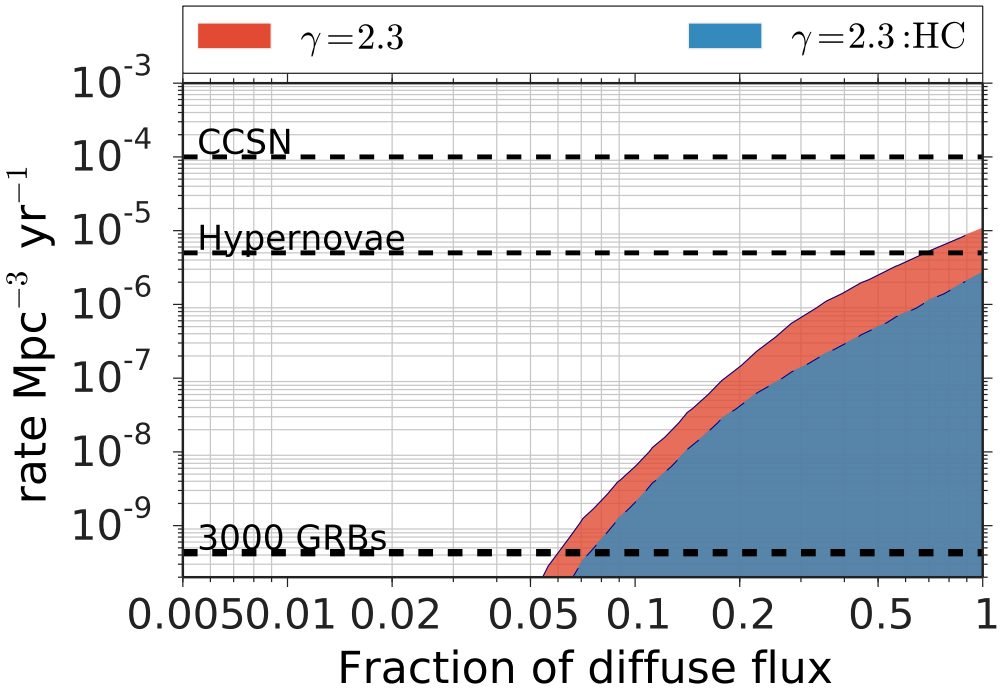

Figure 22: Limits on the contribution of short transient sources to the HESE flux depending on their rate density. The 90% confidence regions are shown for a spectrum with $\gamma = 2.3$ comparing the WP and the HC model.

In case of the higher multiplets, the signal contribution is similar dependent on the low luminosity GRBs (Fig. 20b) and even more so on the close ones (Fig. 20d). However, while the behavior so far differed quite obviously from the distribution produced with the WP model, the possibility to detect a neutrino multiplet depends similarly on close by GRBs (compare Figs. 20d and 20c). Keeping in mind that most of the signal is generated by multiplets within a redshift of one for both the WP model (Fig 21a) and the HC model (Fig. 21b), the comparatively small difference of a factor of 1.28 between the two points of 90% confidence level assuming 3000 GRBs per year is explained. The lack of high luminosity GRBs in the HC model does not matter, as the signal depends mainly on GRBs close enough to produce enough higher multiplets. The discrepancy between the two models increase slightly towards higher GRB rate densities with less flux per GRB. While the flux decrease can be compensated to a degree by the high luminosity GRBs, this is not possible for the HC model.

In conclusion it is possible to say that the limits for do only depend partially on the luminosity function. The limits on the HC model are mainly produced by the low luminosity GRBs due to the lack of high luminosity ones. This leads to worse limits in comparison to the WP model. However, the discrepancy is contained due to the dependence on multiplets from close by GRBs. Both models still exclude a wide region of parameter space.

7.2.2 Supernova Luminosity Function

Examining a different luminosity distribution in the previous section was interesting, as a big variation of the luminosity could lead to the one very bright GRB to be detected. Limiting the number of high luminosity GRBs worsened the limits but a wide range of the parameter space could still be ruled out. Continuing the process one could slim down the luminosity distribution until only a delta function remains. The SN luminosity function (Eq. ???) is a step in that direction with a Gaussian with width ???. The average luminosity is higher than a lot of values from the WP or HC models, however, it is very unlikely to have GRBs with very high luminosities.

SNe are especially interesting because using the WP model and a spectrum with $\gamma = 2.7$, the limits extend

from rate densities that are likely for GRBs to very high values and reaching the population of Core Collapse SNe. According to ???, some SNe could create jets similar to GRBs producing high energy neutrinos. Considering that not all SNe might have a jet and that we could only see them if the jet pointed towards earth, one has to look at the parameter space at possibly a hundredth or less than the actual SN rate density making the limits even more stringent. Using the same redshift distribution as motivated in Section ??? and the luminosity distribution (Eq. ???) chosen to represent the SNe population, the limits worsen but still exclude the possibility that SNe contribute the complete measured high energy neutrino flux (Fig. 23). However, this depends on choosing the most optimistic fit to the measured HESE flux with $\gamma = 2.7$ (Eq. ???). Using a harder spectrum decreases the chance of ruling out SNe as the main source.

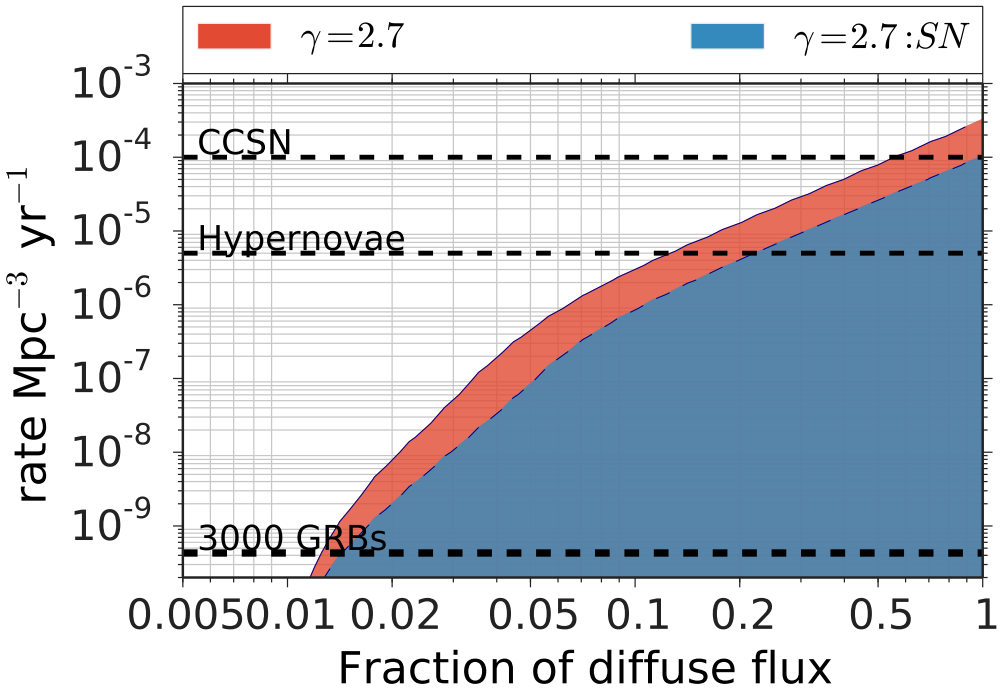

Figure 23: Limits on the contribution of short transient sources to the HESE flux depending on their rate density. The 90% confidence regions are shown for a spectrum with $\gamma = 2.7$ comparing the WP model to a more SN like luminosity distribution.

7.2.3 Low Energy Cut-Off

This section examines the influence low energy cut-off, the minimal energy neutrinos have at source (Eq. ???) that arises in the flux calculation (Eq. ???). As explained in section ???, the absolute normalization of the flux does not change but stays the same when using the same spectrum. However, if the cut-off is high enough, no low energy neutrino is available to form multiplets reducing the likelihood of detection.

The lowest measured energy of the HESE events was 30 TeV. Setting $\hat{E}_{\text{min}}$ to 100 TeV, no OFU singlet with energies lower than ??? GeV should contribute (??? line in Fig. ???). The impact on the signal is more pronounced for the softer spectra, as they predict more events at lower energies (Fig. ???). Using the spectrum with $\gamma = 2.3$, the limits worsen drastically and are in the range of the spectrum with $\gamma = 2$ with an exponential cut-off (Fig. 24).

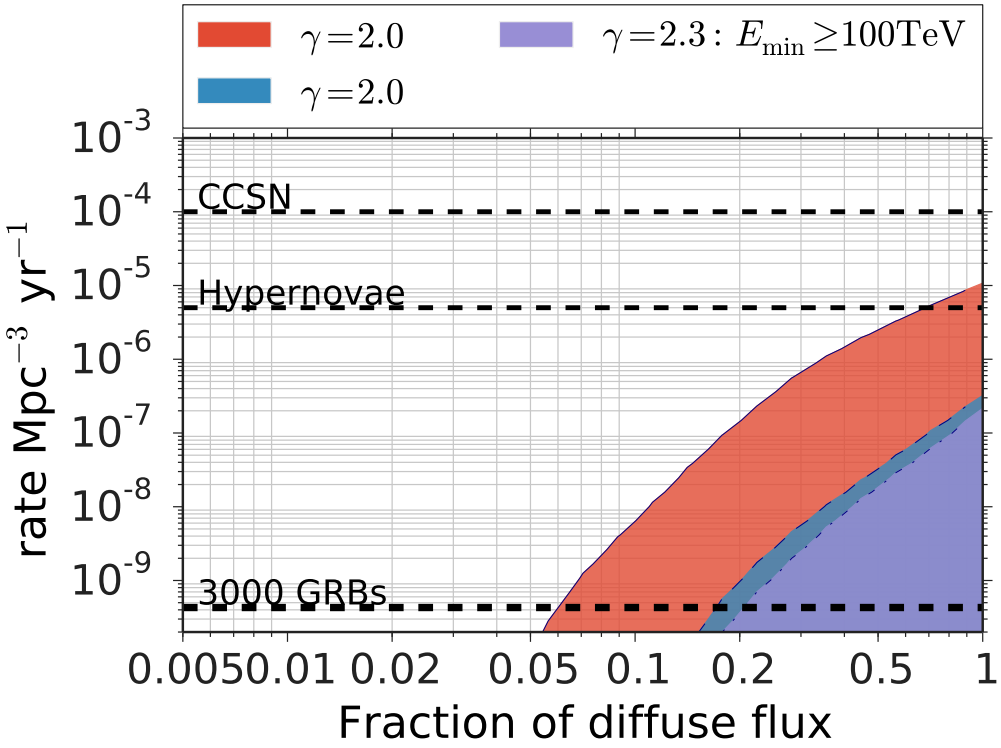

Figure 24: Limits on the contribution of short transient sources to the HESE flux depending on their rate density. The 90% confidence regions are shown for a spectrum with $\gamma = 2.3$ and $\gamma = 2$ comparing them to a spectrum with $\gamma = 2.3$ and a minimal neutrino energy at source of 100 TeV.

References

[1] S. Ando and J. F. Beacom. Revealing the Supernova Gamma-Ray Burst Connection with TeV Neutrinos. *Physical Review Letters*, 95(6):061103, August 2005.

[2] E. J. Howell, D. M. Coward, G. Stratta, B. Gendre, and H. Zhou. Constraining the rate and luminosity function of Swift gamma-ray bursts. , 444:15–28, October 2014.

[3] K. Murase and K. Ioka. TeV-PeV Neutrinos from Low-Power Gamma-Ray Burst Jets inside Stars. *Physical Review Letters*, 111(12):121102, September 2013.

[4] D. Wanderman and T. Piran. The luminosity function and the rate of Swift's gamma-ray bursts. , 406:1944–1958, August 2010.